Monthly Notices
of the
ROYAL ASTRONOMICAL SOCIETY

Mon. Not. R. Astron. Soc. **418,** 2054–2073 (2011) doi:10.1111/j.1365-2966.2011.19625.x

On the mass-to-light ratios of fossil groups. Are they simply dark clusters?

Robert N. Proctor,[1⋆] Claudia Mendes de Oliveira,[1] Renato Dupke,[2,3,4] Raimundo Lopes de Oliveira,[5,6] Eduardo S. Cypriano,[1] Eric D. Miller[7] and Eli Rykoff[8]

[1]*Universidade de São Paulo, IAG, Rua do Matão, 1226, São Paulo 05508-900, Brazil*
[2]*University of Michigan, Ann Arbor, MI 48109, USA*
[3]*Eureka Scientific Inc., Oakland, CA 94602-3017, USA*
[4]*Observatório Nacional, Rua Gal. José Cristino, 20921-400 Rio de Janeiro, Brazil*
[5]*Universidade de São Paulo, Instituto de Física de São Carlos, Caixa Postal 369, 13560-970 São Carlos, SP, Brazil*
[6]*Departamento de Física, Universidade Federal de Sergipe, Av. Marechal Rondon s/n, 49100-000 São Cristóvão, SE, Brazil*
[7]*Kavli Institute for Astrophysics and Space Research, Massachusetts Institute of Technology, Cambridge, MA 02139, USA*
[8]*E. O. Lawrence Berkeley National Lab, 1 Cyclotron Rd. Berkeley, CA 94720, USA*

Accepted 2011 August 11. Received 2011 August 5; in original form 2011 March 30

ABSTRACT

Defined as X-ray bright galaxy groups with large differences between the luminosities of their brightest and second brightest galaxies, 'fossil groups' are believed to be some of the oldest galaxy systems in the Universe. They have therefore been the subject of much recent research.

In this work we present a study of 10 fossil group candidates with an average of 33 spectroscopically confirmed members per group, making this the deepest study of its type to date. We also use these data to perform an analysis of the luminosity function of our sample of fossil groups.

We confirm the high masses previously reported for many of fossil systems, finding values more similar to those of clusters than of groups. We also confirm the high dynamical mass-to-light ratios reported in many previous studies. While our results are consistent with previous studies in many ways, our interpretation is not. This is because we show that, while the luminosities of the bright central galaxies (BCGs) in these systems are consistent with their high dynamical masses, their richnesses (total number of galaxies above some canonical value) are extremely low. This leads us to suggest a new interpretation of fossil systems in which the large differences between the luminosities of their brightest and second brightest galaxies are simply the result of the high BCG luminosities and low richnesses, while the high masses and low richnesses also explain the high mass-to-light ratios. Our results therefore suggest that fossil systems can be characterized as cluster-like in their masses and BCG luminosities, but possessing the richnesses and optical luminosities of relatively poor groups. These findings are not predicted by any of the current models for the formation of fossil groups. Therefore, if this picture is confirmed, current ideas about the formation and evolution of fossil systems will need to be reformulated.

Key words: galaxies: clusters: general – galaxies: groups: general – X-rays: galaxies: clusters.

1 INTRODUCTION

The study of galaxy groups and clusters has become a powerful tool in many aspects of astrophysical research. From the cosmological perspective, groups and clusters mark the most overdense regions of the matter distribution. They can therefore be used to constrain cosmological parameters such as Ω_m, σ_8 and w (the equation of state of dark energy).

From the galaxy formation and evolution perspective, the low velocity dispersions in galaxy groups result in frequent strong interactions between galaxies (i.e. tidal disruption and merging). The high velocity dispersions in clusters, on the other hand, suppress strong interactions between galaxies. However, the deeper potential wells and higher velocities in clusters mean that interactions with the ambient environment (the cluster potential and the intracluster

⋆E-mail: rproctor@astro.iag.usp.br

medium) increase in importance, giving rise to processes such as ram-pressure stripping and strangulation (e.g. Gunn & Gott 1972; Fujita 2004; Rasmussen, Ponman & Mulchaey 2006; Kawata & Mulchaey 2008).

Groups and clusters therefore provide an important testing ground for models of galaxy formation and evolution, as well as enabling the constraint of cosmological parameters. Consequently, there is an ongoing effort to identify and characterize clusters and groups in both the local Universe and, more recently, at higher redshifts (Bauer et al. 2011; Hilton et al. 2010; Strazzullo et al. 2010).

A special class of groups/clusters, first identified by Ponman et al. (1994), is comprised of 'fossil groups' (FGs). These are defined as X-ray luminous structures ($L_X > 5 \times 10^{41}\, h_{70}^{-2}$ erg s^{-1}) with a greater than 2-mag gap between the brightest and the second brightest galaxies within half the virial radius (Jones et al. 2003). Fossil groups are therefore dominated by a massive central early-type galaxy surrounded by a swarm of much smaller galaxies and enclosed in a hot X-ray halo.

The most commonly quoted scenario for the formation of such systems is that, as a result of having remained relatively undisturbed for a significant fraction of a Hubble time, dynamical friction has had time to cause any large galaxies close to the central regions of the group to spiral inwards, ultimately to merge with the central galaxy (D'Onghia et al. 2005; Dariush et al. 2007). This process simultaneously increases the luminosity of the central galaxy and depletes the central regions of massive (bright) galaxies, thus creating the large luminosity gap which, by definition, characterizes FGs. However, there is as yet no direct evidence for this scenario. Consequently, there is to date no consensus on the formation mechanism.

In an effort to address this issue, a few previous studies have investigated the dynamical, X-ray and optical scaling relations of fossil groups (e.g. Vikhlinin et al. 1999; Jones et al. 2003; Yoshioka et al. 2004; Khosroshahi, Ponman & Jones 2007, hereafter KPJ07; Voevodkin et al. 2010). Many find FGs to be more X-ray luminous than non-fossil groups of the same optical luminosity, while still following the same L_X–T_X relation. This results in most of these studies finding fossils to have very high mass-to-light ratios. Each of these studies is at pains to point out that this is consistent with their early formation – regardless of their preferred formation mechanism. There are, however, two works in the literature (Voevodkin et al. 2010; Aguerri et al. 2011) that refute this X-ray excess. Voevodkin et al. (2010) claim instead that 'the X-ray brightness of massive fossil systems is consistent with that of the general population of galaxy clusters and follows the same L_X–L_{opt} scaling relation'. However, in a recent re-examination of their data Voevodkin et al. found a serious error in their estimations of the optical luminosities (private communication). So Voevodkin et al. agreed that their finding is invalid. In the case of Aguerri et al. (2011) the single system reported is at a redshift of 0.5 and possesses a mass significantly larger than any previously reported fossil system. In addition, Aguerri et al. report only a lower limit on the mass-to-light ratio of the system. These issues make a meaningful comparison with the low-redshift systems in the literature problematic. The general consensus therefore remains that fossil systems exhibit high mass-to-light ratios.

In this paper we present an analysis of the dynamical, X-ray and optical properties of 10 fossil groups (five new and five previously reported in the literature). Our study is similar to that of KPJ07. However, due to our deeper spectroscopy, our sample comprises an average of 33 galaxies per group, compared to ∼10 in KPJ07. The large number of galaxies per group in our study also allows us to look for spatiodynamic substructure in our sample. In the course of our analysis we also critically examine the criteria used in the literature in determining whether systems are fossil or not, and compare them to the original definition of Jones et al. (2003).

The paper is organized out as follows. In Section 2 we describe the sample selection, observations, data reductions and supplementary data. Section 3 details our methods of analysis. In Section 4 our results are presented and discussed. In Section 5 we summarize our results and discuss issues arising from them. Our conclusions are presented in Section 6.

Unless otherwise stated, all data presented in this work are scaled to a cosmology with a Hubble constant of 70 km s^{-1} Mpc^{-1}, $\Omega_M = 0.3$ and $\Omega_\Lambda = 0.7$.

2 SAMPLE SELECTION, OBSERVATIONS AND DATA REDUCTIONS

2.1 Sample selection

Five of the groups reported in this paper were selected from the Sloan Digital Sky Survey (SDSS) maxBCG[1] catalogue (Koester et al. 2007). We will refer to these groups as the 'SDSS sample'.

The maxBCG algorithm identifies clusters as overdensities of red galaxies. In the construction of the catalogue, the richness of each cluster is initially estimated as N_{gal}, which is approximately the number of red sequence galaxies within $\pm 2\sigma$ of the $g - r$ colour of the BCG within a fixed 1 h^{-1} Mpc aperture. The initial richness estimate (N_{gal}) is then used to derive a scaled aperture (Hansen et al. 2005) and the remeasured richness is called N_{200}. Note, however, that although N_{200} is an effective tracer of mass (e.g. Becker et al. 2007; Johnston et al. 2007; Rykoff et al. 2008; Rozo et al. 2009), it is not actually a measure of the number of galaxies within R_{200}, since the values of R_{200} were not defined in these works.

Now, given that the definition of fossil groups involves the gap between the first- and second-ranked galaxies within $0.5R_{200}$, it is clearly crucial that, for this work, we have an accurate measure of R_{200}. For the purposes of our study we therefore adopt the value of R_{200} obtained using the weak lensing analysis of Johnston et al. (2007) and Sheldon et al. (2009). In these studies, the maxBCG systems were stacked in bins of N_{200} (as defined above) in order to measure M_{200} and R_{200}. Throughout this work we refer to the R_{200} radius derived in this way as $R_{200,S}$.

The sample presented here was selected from low-richness clusters ($9 < N_{200} < 25$; see Miller et al. 2011) and was required to exhibit an i-band magnitude gap of $\geq$2 mag between the first- and second-ranked galaxies within $0.5R_{200}$ (as defined above) of the group centre. The brightest group/cluster galaxy (BCG) was required to be brighter than $9 \times 10^{10}\, L_\odot$ (with the luminosity data k-corrected to $z = 0.25$) and in the redshift range $0.1 < z < 0.15$. Groups whose BCG exhibited evidence for a bright active galactic nucleus (AGN) at the core were excluded in order to maximize the utility of the low spatial resolution *XMM–Newton* follow-up that is a part of the programme.

Within each group individual galaxies were then priorities for spectroscopic observation on the Magellan Baade telescope. Prioritization was performed by preferentially selecting galaxies within 500 kpc of the BCG and brighter than 20 mag in the r band. Despite the preference for galaxies close to the BCG, candidates were selected out to the full extent of the IMACS field of view (∼30 arcmin

[1] Based on DR6 of the SDSS.

or typically ∼4 Mpc). No galaxies fainter than 21 mag in r were selected. Galaxies with $g - i$ colour 0.1-mag redder than the red sequence identified in the maxBCG catalogue were also rejected as likely background galaxies.

A total of ∼90 galaxies were selected in this way for each group, requiring two pointings (masks) per group. The success of the selection scheme is evidenced by the relatively high fraction of galaxies (≥50 per cent) that we confirm to be at the redshift of the central galaxy. However, it should be noted that the scheme results in a sample that is neither photometrically nor spatially complete.

We also report new Gemini GMOS data for the fossil groups RX J1256.0+2556 and RX J1331.5+1108. Pre-imaging of the groups in g and i bands was carried out on 2006 February 2 and 2005 February 19, respectively. Imaging of each group consisted of 3 × 290 s exposures in each waveband. Calibration to the SDSS photometric system was carried out using four stars in the Landolt (1992) field PG1323–086. Spectroscopic candidates were selected on the basis of their apparent magnitudes ($m_i < 21.5$ mag) and their position on the colour–magnitude diagram constructed using galaxies in the vicinity of the group (i.e. only galaxies close to, or bluer than, the red sequence visible in the colour–magnitude relation were selected). A total of 38 and 22 galaxies were selected in this way for RX J1256.0+2556 and RX J1331.5+1108, respectively.

We supplement the above samples with three other fossil groups that have been spectroscopically studied using GMOS as above to depths permitting the identification of 20–40 confirmed members: RX J1340.6+4018, RX J1416.4+2315 and RX J1552.2+2013. These have been previously reported in the literature by Mendes de Oliveira et al. (2009), Cypriano, Mendes de Oliveira & Sodré (2006) and Mendes de Oliveira, Cypriano & Sodré (2006), respectively. We will refer to these five groups (RX J1256.0+2556, RX J1331.5+1108, RX J1340.6+4018, RX J1416.4+2315 and RX J1552.2+2013) as the 'RXJ sample'.

For each group we also include, when available, spectroscopic SDSS data for the observed fields to augment both the literature and new groups. These relatively bright galaxies, which often include the central group galaxies, were generally avoided from our Magellan and Gemini observing plans in order to maximize the number of new group members identified.

It is important to note that the selection criteria for the two samples (SDSS and RXJ) differed. The SDSS sample that possesses bright central galaxies (BCGs) in low-richness groups, as well as meets the magnitude gap criterion, was selected (as described above). The selection criteria of the RXJ sample are a little less well defined, being selected (according to Jones et al. 2003) by a 'variety of indicators'. The selection included only high X-ray luminosity groups with appropriate magnitude gaps and paying 'particular attention' to groups with low ratios of X-ray to BCG optical luminosities and selecting '. . . . . system[s] dominated by a single galaxy'. These selection criteria were nominally designed to reflect the properties of the prototypical fossil group (RX J1340.6+4018) first reported by Ponman et al. (1994). We will consider the impact of these differing selection criteria in a later section.

2.2 Spectroscopic observations

The Magellan Baade telescope multi-object spectroscopy of five candidate fossil groups selected from the maxBCG catalogue was carried out on the f/2 camera of the IMACS instrument in 2009 February. The 300 lines mm^{-1} grating was used in conjunction with the 'Spectroscopic 2' filter in order to maximize the number of spectra that could be fitted on to the CCD. A slitwidth of 1.0 arcsec was used for all the galaxies. The resultant spectra covered the 4800–8000 Å spectral range at a resolution of ∼6.5 Å and a dispersion of 2.6 Å pixel^{-1} (with ×2 spectral binning). The ∼30 arcmin field-of-view results in a spatial extent of >4 Mpc at the redshifts of these groups. Two 1800-s observations of two masks were carried out for each group.

The Gemini GMOS spectroscopic observations of RX J1256.0+2556 were carried out on Gemini North on 2006 June 24 (programme ID GN-2006A-Q-31). Observations of RX J1331.5+1108 were carried out on Gemini North on 2005 March 7 (GN-2005A-Q-38). Observations were carried out using the R400 grating and slits of 1-arcsec width, giving a resolution of 6.5 Å over 4000–8000 Å. Three exposures of 2400 s were performed. It should be noted that the field-of-view of the GMOS instrument (∼5.5 × 5.5 arcmin) is considerably smaller than the IMACS instrument on Magellan, resulting in spatial extents of 1.2 and 0.5 Mpc at the redshifts of RX J1256.0+2556 and RX J1331.5+1108, respectively.

2.3 Data reduction

The Magellan data (systems with prefix SDSS in Table 1) were reduced using the COSMOS pipeline provided by the Magellan consortium. However, during the analysis it was discovered that the optical map embedded in the software had not been updated after a change in the CCD configuration. This resulted in step functions in the spectral and spatial maps generated by the software. The problems in the spatial mapping are of no concern for the present work as, for our purposes, they are adequately handled by the pipeline. However, in order to compensate for the spectral distortions, it was found necessary to reposition the data on the CCDs. This process is only accurate to about 0.5 pixels (∼50 km s^{-1}). We therefore assume this value to be a minimum error in individual recession velocity measures. Thereafter, reductions followed a standard procedure of debiasing, flat-fielding, wavelength calibration (using Cu-Ar comparison-lamp exposures), sky-subtraction, cosmic ray removal and extraction using the COSMOS pipeline.[2]

Data reductions of the Gemini spectroscopic data were carried out using the IRAF Gemini package GMOS as described in Mendes de Oliveira et al. (2009). Wavelength calibrations were carried out using Cu-Ar comparison-lamp exposures. Positions and magnitudes were obtained for all objects using the SExtractor program of Bertin & Arnouts (1996).

2.3.1 Measurement of recession velocities

For the Magellan data, recession velocities were measured using the Fourier cross-correlation routine (fxcor) within IRAF. As no velocity standards were observed, a synthetic spectrum of a typical early-type galaxy was used as a template. In order to facilitate the identification of group members, the template was first redshifted by the value of the redshift of the central galaxy of the group in question, as given by the SDSS spectroscopic survey. All the values of recession velocity were therefore measured with respect to the central galaxy.[3]

Only the cross-correlations with unambiguous peaks were accepted as valid measures. However, an inspection of the spectra

[2] http:/obs.carnegiescience.edu/Code/cosmos/Cookbook.html

[3] We note that the $1 + z$ cosmological factor required in the calculation of velocity dispersion at high redshifts is automatically accounted for in this approach.

Table 1. For groups with prefix SDSS (the SDSS sample), X-ray data are the *Chandra* data of Miller et al. (2011). For the systems in the RXJ sample the *Chandra* data of KPJ07 are presented. X-ray luminosities and temperatures are specified for an aperture equal in size to R_{200}. The values of R_{200} used in the selection of the target systems ($R_{200,\mathrm{S}}$) are shown (see text). Values derived from the X-ray data ($R_{200,\mathrm{X}}$) are also presented. For SDSS J0906+0301, which was undetected in the X-ray, the $R_{200,\mathrm{X}}$ is assumed to be 1.0 Mpc based on its dynamical properties (see Section 5.2). In all other cases $R_{200,\mathrm{X}}$ was calculated from the X-ray temperature using equation (2). Group masses derived using equation (3) are also presented.

Group	z	$\log(L_{\mathrm{X}})$ (erg s^{-1})	kT_{X} (keV)	$R_{200,\mathrm{S}}$ (Mpc)	$R_{200,\mathrm{X}}$ (Mpc)	$\log(M_{200,\mathrm{X}})$ ($\mathrm{M}_{\odot}$)
SDSS J0906+0301	0.1359	<43.29	–	0.66	(1.0)*	(14.12 ± 0.25)
SDSS J1045+0420	0.1539	44.01	2.47	0.76	1.19	14.35 ± 0.14
SDSS J1136+0713	0.1030	43.59	2.64	0.86	1.26	14.41 ± 0.23
SDSS J0856+0553	0.0939	43.92	2.73	0.83	1.29	14.43 ± 0.19
SDSS J1017+0156	0.1177	42.99	2.13	0.74	1.12	14.26 ± 0.24
RX J1256.0+2556	0.2327	43.70	2.63	0.69	1.18	14.38 ± 0.20
RX J1331.5+1108	0.0802	42.32	0.81	0.71	0.71	13.65 ± 0.10
RX J1340.5+4017	0.1719	42.72	1.16	0.75	0.81	13.86 ± 0.23
RX J1416.4+2315	0.1381	44.23	4.00	0.93	1.52	14.66 ± 0.10
RX J1552.2+2013	0.1357	43.78	2.85	0.83	1.29	14.45 ± 0.14

*Assumed value.

also revealed a number of galaxies for which unambiguous recession velocities could not be derived using fxcor, but which exhibited strong emission lines. Recession velocities for these galaxies were measured by fitting a Gaussian profile to the Hα emission line. The typical absorption and emission line errors were both $\sim$75 km s^{-1}.

Recession velocity measurements of the Gemini data were performed using the cross-correlation technique implemented in the RVSAO package within IRAF. Several galaxy templates were employed in this analysis with results taken from the template with the strongest cross-correlation peak. Recession velocities were then converted to the rest frame of the central galaxy using

$$V_i = \frac{cz_i - cz_0}{1 + z_0}, \tag{1}$$

where V_i is the recession velocity of the ith galaxy with respect to the BCG, which has redshift z_0.

In order to maximize the number of *new* cluster members in our sample we selected against galaxies with pre-measured recession velocities in the SDSS spectroscopic survey. However, in order to check the consistency of the two data sets, we did observe eight galaxies which were also observed in the SDSS spectroscopic survey (five in the Magellan sample galaxies and three in the Gemini sample of J1256). A comparison of the derived values for these galaxies showed our values to be offset from the SDSS values by -94 ± 35 and -59 ± 35 km s^{-1} in the Magellan and Gemini samples, respectively, giving -81 ± 35 km s^{-1} for the combined sample. We therefore offset our data by -81 km s^{-1} before combining our data with that of the SDSS.

3 SUPPLEMENTARY DATA

As well as the spectroscopic data detailed above, several sources of supplementary data were employed in our analysis.

3.1 X-ray data

The X-ray data for the five new fossil group candidates presented in this work (groups with the prefix 'SDSS') are taken from Miller et al. (2011). The X-ray data for the remainder of the fossil groups included in this work were taken from KPJ07. The data are shown in Table 1.[4] The Miller et al. (2011) data are derived from *Chandra* ACIS–S3 snapshots, while the KPJ07 data are derived from deeper *Chandra* ACIS–S3 observations. We note that the upper-limit of $\log(L_{\mathrm{X}}) < 43.46$ erg s^{-1} for the non-detection of J0906 is still well above the X-ray luminosity criterion for fossil groups [$\log(L_{\mathrm{X}}) > 41.7$ erg s^{-1}]. This group *may* still therefore meet this criterion, and its eligibility as a fossil candidate will be reviewed in a later section.

Table 1 also shows values of R_{200} (which we take in this work to be an approximation for the virial radius). Values of R_{200} are required in both the selection process (in order to determine the luminosity gap between the first- and second-ranked galaxies within $0.5R_{200}$), as well as in the later analysis.

Table 1 presents both the values of R_{200} used in the selection process ($R_{200,\mathrm{S}}$) and those derived from the X-ray temperatures ($R_{200,\mathrm{X}}$). The latter were derived using the full cosmological form of the expression given in Helsdon & Ponman (2003):

$$R_{200,\mathrm{X}} = 1.14\sqrt{T_{\mathrm{X}}}\, h_{50}^{-1}(z)\,\mathrm{Mpc}, \tag{2}$$

where $h_{50}(z) = h_{50}(\Omega_{\mathrm{M}}(1+z)^3 + \Omega_{\Lambda})^{0.5}$ assumes a $\Omega = 1$ universe and the 1.14 coefficient was derived from the results of the N-body/smoothed particle hydrodynamics simulations of Navarro, Frenk & White (1995). The values of $R_{200,\mathrm{X}}$ so derived are given in Table 1. However, J0906 is a non-detection. Consequently, only an upper limit on its X-ray luminosity could be estimated and its X-ray temperature is unconstrained. We have therefore assumed a value of 1 Mpc for $R_{200,\mathrm{X}}$ of this group based on its dynamical properties (see Section 5.2).

An estimate of the masses of the groups can be made directly from the values of $R_{200,\mathrm{X}}$ using

$$M_{200,\mathrm{X}} = \frac{4}{3}\pi R_{200,\mathrm{X}}^3 \,.\, 200 \,.\, \rho_{\mathrm{crit}}(z), \tag{3}$$

[4] Full galaxy identifiers are given here and shown in Table 1, but throughout the remainder of this paper we will refer to them by abbreviated identifiers in the text (e.g. J0906, J1256, etc).

where $\rho_{\rm crit}(z)$ is the critical density at redshift z. The values of $M_{200,\rm X}$ so derived are given in Table 1. Table 1 shows clear discrepancies between the values of $R_{200,\rm S}$ and $R_{200,\rm X}$.

For the RXJ sample (but with the exception of J1340) $R_{200,\rm S}$ was based on relationships between $L_{\rm X}$ and kT, and kT and R_{200} (see Jones et al. 2003, for details). However, for J1256, J1416 and J1552, the *ROSAT* X-ray data, upon which these estimates were based, yielded X-ray luminosities (and therefore R_{200} values) significantly lower than the subsequent, higher resolution *Chandra* data presented in KPJ07. In the case of J1340, no value of R_{200} was quoted in the original Ponman et al. (1994) paper. We therefore estimated $R_{200,\rm S}$ using the *ROSAT* X-ray temperature given in KPJ07 and the equation given in Jones et al. (2003).

In the case of the SDSS sample, $R_{200,\rm S}$ values were based on the results of the weak lensing analysis of Johnston et al. 2007) for which groups were stacked by their richness ($N_{\rm gal}$; see Section 2.1). We will discuss the cause of the discrepancies between $R_{200,\rm S}$ and $R_{200,\rm X}$ values in this sample in a later section.

Unless otherwise specified, throughout this work virial radii are taken to be the $R_{200,\rm X}$ values given in Table 1.

In Fig. 1 we plot a comparison of the $L_{\rm X}$–$T_{\rm X}$ relation for our fossil groups to the literature relation for 'normal' systems. In this figure normal groups are shown as black dots (Osmond & Ponman 2004) and normal clusters as red dots (Wu et al. 1999). The figure shows the fossil groups to be generally consistent with normal systems. However, we note that, as found in many previous studies (e.g. Mendes de Oliveira et al. 2006, 2009; Cypriano et al. 2006; KPJ07), a significant number of the fossil groups exhibit values consistent with *clusters* rather than groups. However, there are four systems with group-like X-ray properties. Interestingly, these appear to lie above the $L_{\rm X}$–$T_{\rm X}$ relation for normal groups. We will comment further on these trends in a later section.

3.2 Control samples from the literature

Our analysis involve the comparison of our fossil group candidates with 'normal' systems. The sources for normal groups were taken from the GEMS project of Osmond & Ponman (2004), supplemented by groups from the study of Girardi et al. (2002). For clusters, X-ray luminosities were taken from Wu et al. (1999) and Zhang et al. (2011). X-ray temperatures were taken from Wu et al. (1999) and r-band luminosities from Girardi et al. (2002). However, we note that, these studies were not specifically selected to possess low m_{12} values. The samples *likely* therefore contain a few systems that we would consider fossil systems.

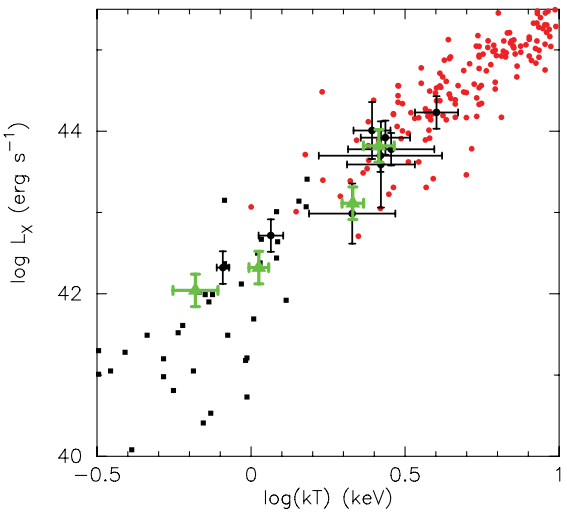

Figure 1. Fossil groups are plotted in the $L_{\rm X}$–$T_{\rm X}$ plane and compared to literature values for 'normal' systems. Literature values for normal clusters (Wu, Xue & Fang 1999) are shown as red dots, while literature values for normal groups (Osmond & Ponman 2004) are shown as black squares. Fossils taken from KPJ07 are shown as green squares. The fossil groups analysed in this work are shown as black dots (with error bars).

When converting galaxy luminosities from the literature to the r band used in this work, values of $B-R, B-r$ and $r-i$ were taken to be 1.57, 1.33 and 0.4 mag, respectively. To convert absolute magnitudes into solar luminosities, values of the solar B, R, r and i band absolute magnitudes were taken to be 5.48, 4.42, 4.76 and 4.58 mag, respectively. Finally, the value of $B_j - B$ in galaxies was taken to be the solar value when converting the Girardi et al. (2002) luminosities to Sloan r band.

All literature values were converted to the $H_0 = 70\,{\rm km\,s^{-1}\,Mpc^{-1}}$, $\Omega_{\rm M} = 0.3$, $\Omega_\Lambda = 0.7$ cosmology used throughout this paper.

4 ANALYSIS

In this section we detail each of the elements of our analyses of the spectroscopic and photometric data. The data are presented in Appendix B.

4.1 Group velocities and velocity dispersions

In this section we detail our estimates of group velocities, velocity dispersions and dynamical virial radii (i.e. $R_{200,\rm dyn}$) of the fossil groups.

The average velocity of the group was also calculated as

$$RV_{\rm group} = \frac{\Sigma V_i}{N} \pm \frac{\sigma_{200}}{\sqrt{N}}\ {\rm km\,s^{-1}}, \tag{4}$$

where V_i is the recession velocity of the ith galaxy within $R_{200,\rm X}$ and N is the total number of non-BCG galaxies within $R_{200,\rm X}$ (BCG is excluded from this calculation). The offset of BCG with respect to the group average ($\Delta RV_{\rm BCG} = {\rm RV_{BCG}} - RV_{\rm group}$) was then calculated (Table 2). The velocity dispersion (σ_{200}) of each group was estimated from the recession velocities by

$$\sigma_{200} = \sqrt{\frac{\Sigma(V_i - RV_{\rm group})^2}{N-1}} \pm \frac{\sigma_{200}}{\sqrt{2(N-1)}}\ {\rm km\,s^{-1}}. \tag{5}$$

Both of the above definitions require an estimate of R_{200}. For these estimates, and generally throughout this work, we use the values derived from the X-ray temperature as described in Section 3.1 and given in Table 1. However, for comparison purposes we also make virial radius estimates based on the observed velocity dispersion (which we will refer to as *dynamical* virial radius).

4.2 Dynamical virial radii

Dynamical virial radii can be estimated from kinematic data using expressions which express the virial radius as being proportional to the velocity dispersion. From the virial theorem, Carlberg et al. (1997) derived an expression for R_{200}:

$$R_{200,\rm dyn} = \frac{\sqrt{3}\sigma_{200}}{10H(z)}\ {\rm Mpc}, \tag{6}$$

where σ_{200} is the velocity dispersion of galaxies within $R_{200,\rm X}$ as defined above, and $H(z)$ is the Hubble constant at redshift of the group. Alternatively, Girardi et al. (1998) use both virial theory *and*

Table 2. Dynamical data derived within $R_{200,X}$. The table shows n – the number of galaxies within $R_{200,X}$ (with the number of galaxies taken from the SDSS in brackets), the estimated velocity dispersions and the offset of the BCG velocity with respect to the group average (ΔRV_{BCG}). $R_{200,dyn}$ and masses estimated from equations (6) and (8) are also presented. Errors in σ and ΔRV_{BCG} were calculated according to equations (5) and (4) and were propagated through equations (6) and (8) for $R_{200,dyn}$ and $M_{200,dyn}$.

Group	n	σ (km s^{-1})	ΔRV_{BCG} (km s^{-1})	$R_{200,dyn}$ (Mpc)	$\log(M_{200,dyn})$ ($M_\odot$)
SDSS J0906	25 (1)	506 ± 72	-154 ± 103	1.17 ± 0.16	14.25 ± 0.21
SDSS J1045	38 (2)	664 ± 77	-69 ± 109	1.52 ± 0.18	14.58 ± 0.13
SDSS J1136	45 (2)	490 ± 52	11 ± 74	1.15 ± 0.12	14.30 ± 0.22
SDSS J0856	63 (17)	478 ± 43	-24 ± 61	1.13 ± 0.11	14.26 ± 0.16
SDSS J1017	23 (1)	474 ± 71	73 ± 101	1.11 ± 0.17	14.23 ± 0.29
RXJ J1256	28 (1)	622 ± 84	159 ± 120	1.37 ± 0.19	14.50 ± 0.40
RXJ J1331	10 (6)	338 ± 77	-142 ± 111	0.80 ± 0.18	13.74 ± 0.25
RXJ J1340	22 (2)	537 ± 82	-34 ± 117	1.22 ± 0.19	14.21 ± 0.10
RXJ J1416	40 (11)	815 ± 87	285 ± 124	1.89 ± 0.20	14.85 ± 0.15
RXJ J1552	35 (8)	803 ± 96	43 ± 138	1.86 ± 0.23	14.76 ± 0.28

observational data to derive an expression for the virial radius (at unstated overdensity):

$$R_{\rm vir,dyn} = \frac{0.2\sigma_{200}}{H_0}\ {\rm Mpc}. \quad (7)$$

Both of the above equations are directly proportional to the velocity dispersion, and differ only in the constants of proportionality [with the Girardi et al. (1998) values larger by a factor of ∼15 per cent]. We therefore use equation (6) above for estimates of the dynamical virial radii and leave it to the reader to apply the ∼15 per cent offset if the Girardi et al. (1998) values are required.

4.3 Dynamical masses

We also make estimates of the dynamical mass within $R_{200,X}$ of each group or cluster using our dynamical data. These are calculated using the expression (Ramella et al. 2004)

$$M_{200,\rm dyn} = \frac{3}{G}\sigma_{200}^2 R_{200,X}, \quad (8)$$

which can be expressed in the more convenient form

$$M_{200,\rm dyn} = 6.975 \left(\frac{\sigma_{200}}{1000\,{\rm km\,s^{-1}}}\right)^2 \left(\frac{R_{200,X}}{1\,{\rm Mpc}}\right) \times 10^{14}\,{\rm M_\odot}, \quad (9)$$

where $R_{200,X}$ is calculated using equation (2).

4.4 Composite luminosity function

The spectroscopy for the fossil candidates in this paper obtained using the Magellan telescope (i.e. the SDSS sample) covers a significant radial extent in each system (i.e $>R_{200,X}$). This allows the accurate determination of the luminosity function (LF) of galaxies within $R_{200,X}$ in these systems. Although a few determinations of the LF of individual fossil groups have been attempted in the literature (Mendes de Oliveira et al. 2006, 2009, for J1552 and J1340 and Cypriano et al. 2006, for J1416), those were within radii smaller than $R_{200,X}$. This is therefore the first determination of the LF of fossil groups which include more than 30 galaxies per group and reach out to $R_{200,X}$.

To calculate the LF of each group, we considered all the galaxies inside a projected radius corresponding to $R_{200,X}$ of the group. This requires the determination of the selection function $S(m')$ in each group in order to estimate the completeness of the spectroscopy. This was done using the following equation:

$$S(m') = \frac{\#GAL_z(m')}{\#GAL(m')}\ , \quad (10)$$

where $\#GAL_z(m')$ is the total number of galaxies with known spectroscopic redshifts, being member galaxies or not, and $\#GAL(m')$ is the total number of galaxies in the region as identified via photometry (from SDSS), in both cases for galaxies with magnitude m such that $|m - m'| < \Delta m$. Membership to the group was defined in the velocity range within 2000 km s^{-1} from the velocity of the central galaxy and within $R_{200,X}$ of the position of the central galaxy. Then the LF is defined by

$$LF(m') = \frac{\#GAL_{z,\rm grp}(m')}{S(m')}, \quad (11)$$

where $\#GAL_{z,\rm grp}(m')$ is the number of member galaxies as determined by spectroscopy.

Thus, the individual LF for each group in a given band was obtained by simply dividing the number of galaxies in each bin of absolute magnitude by the completeness fraction. The second step was then to construct the composite LF by averaging, bin per bin, the individual LFs of each of the five groups for each band g, r and i.

Finally the galaxy distributions were fitted by the Schechter function (Schechter 1976).

4.5 Total optical luminosities

Part of our analysis considers the total optical luminosities of the groups.

For the SDSS sample, which was well sampled out to R_{200}, and for which the selection functions and completeness were estimated during the construction of the composite LF, we estimate the total optical luminosities using completeness-corrected data.

For the RXJ sample a more complex procedure was adopted, since composite LFs were not available and our spectroscopic data are only well sampled within $0.7R_{200}$. However, our use of the data from the SDSS data base means that both RXJ and SDSS samples are 100 per cent complete all the way out to R_{200} down to an apparent magnitude of 17.7 (an absolute magnitude of approximately –21 at the redshift of our groups). We therefore use the SDSS sample

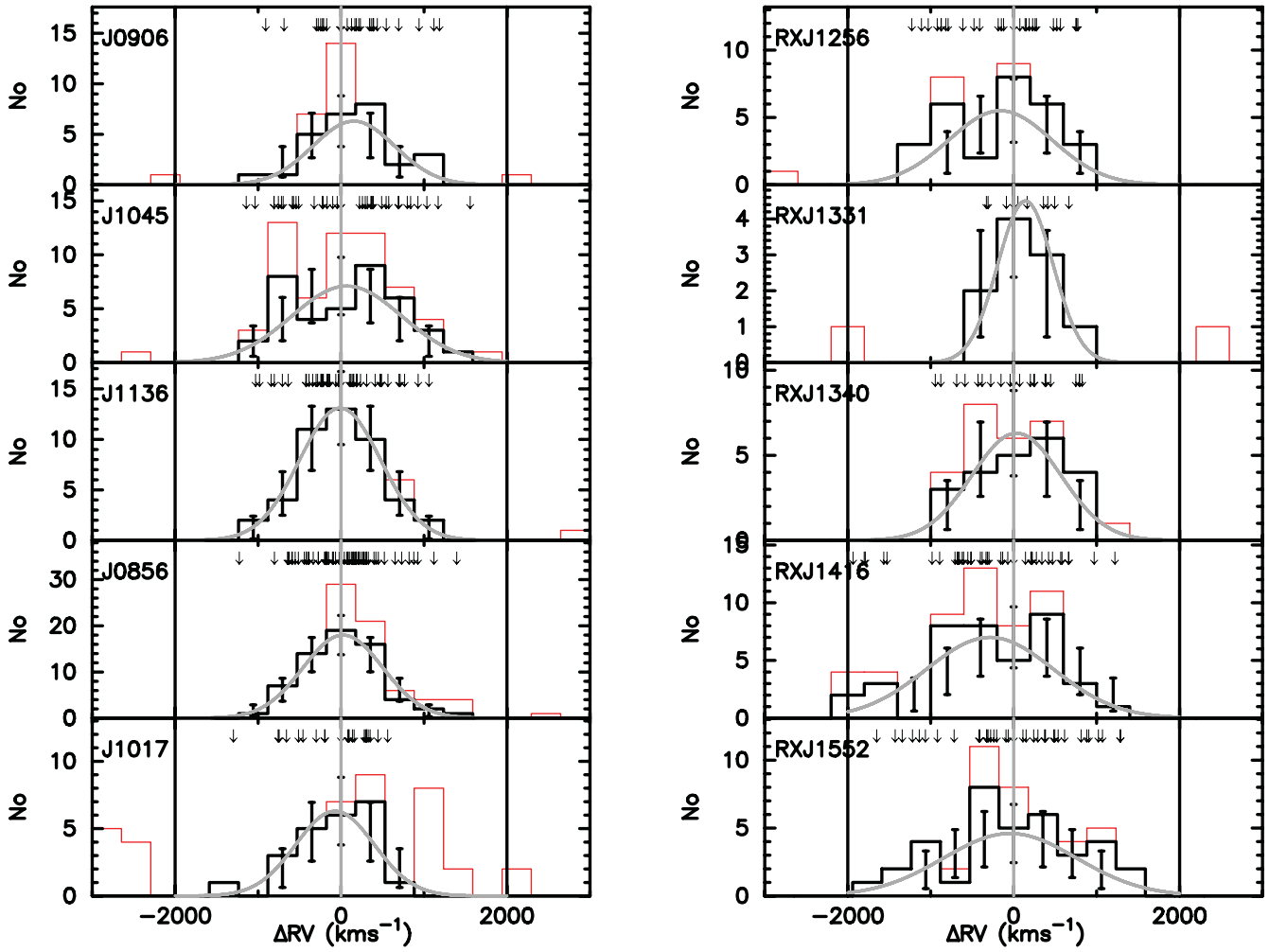

Figure 2. Distributions of recession velocities about the average group velocity. Arrows mark the recession velocities of individual galaxies. Vertical black lines represent the 2000 km s^{-1} velocity limit of group members applied to all groups. Vertical grey lines represent the velocities of the BCG in each group ($\Delta RV_{\rm BCG}$, Table 2). Histograms in black include all the member galaxies within $R_{200,\rm X}$. The red histograms show galaxies outside the velocity or radius limits. Gaussian distributions matching the recession velocity distributions (i.e. assuming the velocity dispersions listed in Table 2) are shown as grey lines with Poisson errors to aid in assessing the significance of apparent velocity substructure. Significant asymmetries and/or discontinuities are visible in the distributions of J1017, J1256 and J1416.

to estimate the effect on the total luminosity of the poor spatial sampling and completeness in the RXJ sample.

We begin by simply adding the optical luminosities of all the identified group members. Now, in the SDSS groups, ∼20 per cent of the galaxies below an apparent magnitude of 17.7 lie between $0.7R_{200}$ and R_{200}. For each RXJ group, we therefore added to the total luminosity 25 per cent of the light in galaxies that are fainter than this limit and lie within $0.7R_{200}$. This increases the logarithmic luminosity estimates by ∼0.03 dex (with a range of 0.01–0.04 dex). We then assumed that the completeness of each group in the RXJ sample was the same as the average of the SDSS sample. This further increases the luminosity estimates by ∼0.07 dex (with a range of 0.04–0.1 dex).

5 RESULTS

In this section we detail the results of our analysis. The recession velocities and apparent magnitudes of all new data presented in this paper are given in Appendix B. We begin by considering the results of our kinematic analysis.

5.1 Recession velocities

The distributions of the recession velocities of galaxies within ∼3 Mpc of the central galaxy are shown in Fig. 2. This figure shows that the majority of the groups exhibit recession velocity distributions that are clearly delineated, and near symmetric about zero velocity (i.e. the average velocity of the group). However, there are indications of skew distributions and gaps in the recession velocity distributions in a few cases. Other possible signs of disturbance or background contamination that were considered were large offsets in BCG velocity (Table 2), and spatial groupings of galaxies with similar recession velocities, In order to measure gaps and skewness, we preformed an analysis using the ROSTAT software of Beers, Flynn & Gebhardt (1990). The results of this analysis were then combined with the BCG velocity offsets and a visual inspection for spatial groupings. In three cases (J1017, J1256 and J1416) the groups exhibited positive signs from three of the four criteria listed above. We therefore took these groups as being the most likely to be either contaminated by foreground/background structures or out of equilibrium (i.e. are unvirialized). These groups were therefore

used to test the possible affects of these apparent irregularities on our derived velocity dispersions and dynamical virial radii.

The analysis is presented in detail in Appendix A. In brief, while hints of substructure in the spatial and kinematic data can be seen in a number of systems, the relatively low numbers of members and incomplete spatial coverage of our data preclude definitive statements about the dynamical status of these systems. In our analysis we therefore simply estimated the magnitudes of the effects such substructure, if real, might have on our derived parameters for the three most obvious potential cases. We find that while small quantitative effects may be present, these do not *qualitatively* affect our results. We therefore continue to use the values derived from all the galaxies observed within $R_{200,\mathrm{X}}$ throughout this work. Clearly, follow-up observations of these systems to improve the spatial coverage and depth of spectroscopically confirmed memberships are highly desirable.

5.2 Dynamical properties

The dynamical properties (velocity dispersions, average group velocities, dynamical R_{200} values and dynamical masses) are presented in Table 2.

A comparison of our velocity dispersion results with those of KPJ07, for the four systems common to both studies, shows them to be consistent with our results exhibiting an offset and rms of $+54$ and $104\,\mathrm{km\,s^{-1}}$ with respect to KPJ07. These are easily within 1σ in all cases. Comparison of the log(mass) estimates within R_{200} are also consistent with our results exhibiting an offset and rms of -0.02 and 0.23 dex, respectively. These values are also consistent with the masses derived solely from the X-ray temperature given in Table 1, exhibiting an average offset of only $+0.1$ dex (i.e within 1σ). This clearly shows that the relationship between the values of kT_{X} and velocity dispersion presented in this work is in general consistent with virial theory.

A comparison of the dynamical R_{200} with the X-ray derived values given in Table 1 shows a good agreement, with the dynamical values being on average 0.21 Mpc (18 per cent) larger than the X-ray values with an rms scatter of 0.20 Mpc (18 per cent). Use of the Girardi et al. (1998) expression (equation 7) would have resulted in values still $\sim$15 per cent larger.

A striking feature of the dynamical data is the magnitude of the velocity dispersion and associated mass estimates. The derived masses are, in all but one or two cases, greater than $10^{14}\,\mathrm{M}_{\odot}$. These masses are more consistent with poor *clusters* than with groups – in accordance with the trend suggested by the X-ray luminosities and temperatures (Section 3.1). It should be noted that the two systems with the lowest masses (J1331 and J1340) are the systems identified as possessing low X-ray temperatures and luminosities in Fig. 1.

The data therefore indicate a consistency between the dynamical and X-ray properties. We therefore next consider the scaling relations that relate the dynamical, X-ray and optical properties of groups and clusters.

5.3 Scaling relations

The optical data are presented in Table 3, while the scaling relations are shown in Fig. 3. In this figure the data from the present work are shown as black dots with error bars. We also include the data for three fossil groups from KPJ07. These are shown as green dots with error bars.

The figure also shows values for normal groups and clusters from the literature (as detailed in Section 3.2). It is worth recalling that the normal systems may, in fact, contain some fossil systems, as these were not expressly excluded during the construction of these samples.

The trend noted in the L_{X}–T_{X} plot for the majority of the fossil groups to be more similar to galaxy *clusters* than groups is also evident in the plots of L_{X}–σ and T_{X}–σ of Fig. 3. We therefore find that all three of these commonly used proxies for mass are in agreement, indicating that the majority of the systems in our sample possess masses $\sim 10^{14}\,\mathrm{M}_{\odot}$, or greater. We note that the group that was a non-detection in the X-ray (J0906) has a velocity dispersion of $>500\,\mathrm{km\,s^{-1}}$ ($\log\sigma \sim 2.7$). For the properties of this system to be consistent with our other data, we should expect J0906 to possess a $\log L_{\mathrm{X}} \sim 43.0$. The upper limit of $\log L_{\mathrm{X}} \sim 43.3$ found

Table 3. The richness (N_{200}; see Miller et al. 2011), r-band luminosity of the central galaxies ($L_{r,\mathrm{bcg}}$) and the total r-band luminosities within $R_{200,\mathrm{X}}$ ($L_{r,\mathrm{tot}}$) are given. The luminosity of the BCG is also given as a fraction of the total optical light ($\mathrm{f_{bcg}}$). The magnitude gaps between the first- and second-ranked galaxies within $R_{200,\mathrm{S}}$ – i.e. those used in the selection process – are represented by $m_{12,\mathrm{S}}$, while the magnitude gaps found within $R_{200,\mathrm{X}}$ are represented by $m_{12,\mathrm{X}}$. Finally, the r-band dynamical mass-to-light ratios are presented.

Group	N_{200}	$\log L_{r,\mathrm{bcg}}$ ($\mathrm{L}_{r,\odot}$)	$\log L_{r,\mathrm{tot}}$ ($\mathrm{L}_{r,\odot}$)	$\mathrm{f_{bcg}}$	$m_{12,\mathrm{S}}$ (mag)	$m_{12,\mathrm{X}}$ (mag)	$\log(M_{\mathrm{dyn}}/L_{r,\mathrm{tot}})$ ($\mathrm{M}_{\odot}/\mathrm{L}_{r,\odot}$)
SDSS J0906	9	11.42	11.85	0.38	3.09	3.09	2.40 ± 0.22
SDSS J1045	13	11.44	12.14	0.20	2.00	2.00	2.44 ± 0.16
SDSS J1136	10	11.40	12.10	0.21	2.25	0.58	2.20 ± 0.26
SDSS J0856	16	11.28	12.05	0.18	2.25	1.67	2.21 ± 0.20
SDSS J1017	12	11.37	11.75	0.41	2.72	1.88	2.48 ± 0.29
RXJ J1256*	8	11.15	11.79	0.24	1.53	1.34	2.71 ± 0.41
RXJ J1331	6	10.94	11.41	0.34	1.85	1.85	2.33 ± 0.27
RXJ J1340	8	11.36	11.81	0.36	2.78	1.31	2.40 ± 0.15
RXJ J1416*	28	11.76	12.20	0.35	2.55	2.21	2.65 ± 0.18
RXJ J1552*	19	11.50	12.10	0.25	2.27	1.10	2.66 ± 0.31
Average	13	11.37	11.91	0.29	2.33	1.70	2.45

* The r-band photometry of the galaxies marked by an asterisk was estimated in the i band and converted to the r band using the values given in Section 5.4.

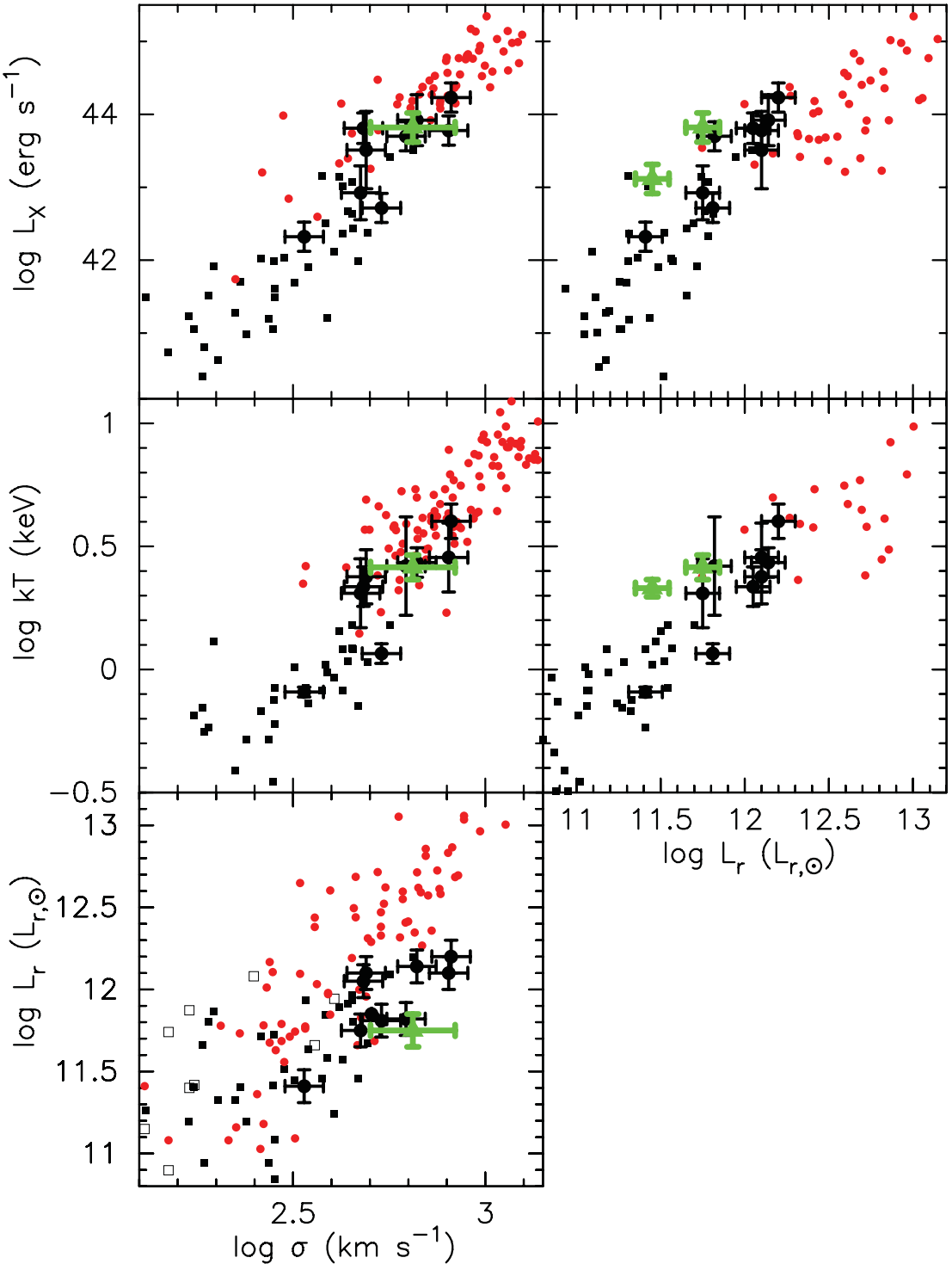

Figure 3. The scaling relations of our sample of fossil groups is compared to normal systems from the literature. The data presented in the paper are shown as black dots with error bars. Three groups from KPJ07 are shown as green dots with error bars. Samples of normal groups are shown as black squares (filled symbols from Osmond & Ponman 2004, and open symbols from Girardi et al. 2002). Clusters are shown as red dots.

for this group therefore does not preclude this system from either meeting the fossil group criteria ($\log L_X > 41.7$), or following the same scaling relations as the remainder of our sample.

However, a severe mismatch with cluster data is evident in the L_r–σ plot, with the fossil groups exhibiting r-band luminosities ∼0.5 dex lower than clusters of the same velocity dispersion. An examination of the L_X–L_r plot of Fig. 3 (top right) shows the fossil groups to lie on the outer envelope of the locus of normal groups. This trend has also been noted in previous works (e.g. Vikhlinin et al. 1999; Jones et al. 2003; KPJ07) and is often interpreted as an X-ray luminosity excess. However, considering the plots with velocity dispersion, it appears that the data are more accurately interpreted as an optical luminosity deficit. Indeed, we note that, if we compensate for the ∼0.5 dex deficit in L_r as suggested by the

L_r–σ plot, then the fossil groups would fall in the cluster region of the L_X–L_r plot.

The disparity in r-band luminosity is harder to discern in the T_X–L_r plot. However, we note that the displacement of the fossil group data points by the ∼0.5 dex suggested by the L_r–σ plot leaves most of the fossil groups consistent with the trends shown by normal cluster-like systems. There are, however, two notable exceptions–J1331 and J1340 (the two systems with the lowest X-ray temperatures), which already exhibit luminosities high for their X-ray temperatures. We note that these groups were also amongst those identified in Fig. 1 as exhibiting low T_X for their L_X. It is therefore possible that these two systems represent a separate, distinct population (i.e. following different scaling relations) from their more massive counterparts. Clearly, an expansion of the data set at low masses (low σ, L_X and T_X) is highly desirable to address this point.

The disparity in r-band luminosity between the majority of the fossil groups and normal systems of the same mass indicates that the mass-to-light ratios of the fossil groups are ∼3 times larger than normal systems of the same mass. This is demonstrated in Table 3 and Fig. 4, in which our mass and mass-to-light ratio values (determined within $R_{200,X}$) are compared to the values for normal systems from Girardi et al. (2002). The Girardi et al. values were estimated within $R_{vir,dyn}$ (equation 7) and are therefore well matched to our data. It is evident from Fig. 4 that the fossil groups lie on or above the highest mass-to-light ratios exhibited by normal systems. It is also interesting to note that the two low-mass fossil systems (J1331 and J1340) also possess high mass-to-light ratios. Therefore, even if these systems do signal the existence of a distinct low-mass population, this too would seem to exhibit high mass-to-light ratios, and their positions in the L_X–T_X, T_X–σ and T_X–L_r planes would suggest low X-ray temperatures for their masses.

We note that our findings (velocity dispersions, masses and total luminosities for the five overlapping systems) are in a good agreement with KPJ07. However, an examination of fig. 10 of KPJ07 suggests that our estimates of mass-to-light ratio are not in agreement with theirs. However, in a recent re-examination of their data (private communication), the authors of KPJ07 discovered that the values of mass used in the construction of their plot were in fact M_{500}, rather than the M_{200} required for the comparison to the Girardi et al. (2002) data. The use of the appropriate mass values would have resulted in their finding considerably higher mass-to-light ratios in the fossil group sample than those in the normal systems represented by the Girardi et al. (2002) data.

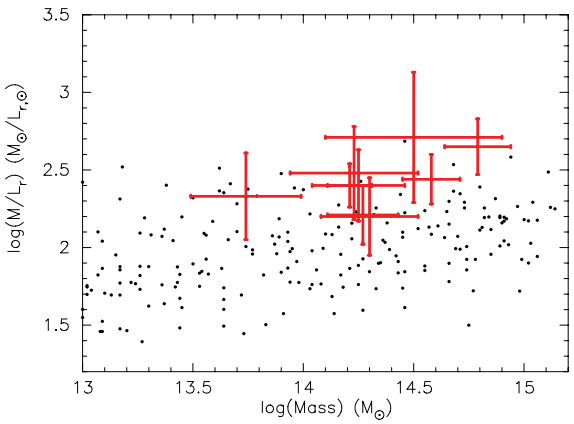

Figure 4. Mass-to-light ratios are plotted against mass (with both parameters estimated within $R_{200,X}$). Literature values for normal groups and clusters (Girardi et al. 2002) are shown as black dots.

To summarize, our consideration of the scaling relations of fossil groups indicates that the most important parameter differentiating the fossil sample from normal systems is their optical luminosity, with Fig. 4 demonstrating that fossil systems possess mass-to-light ratios approximately three times that of normal systems of the same mass. This corresponds to a deficit of *twice* the *total* observed luminosity (including the bright BCGs), or more than three times the total luminosity of *all* the non-BCG galaxies. Such deficits cannot be explained simply by the absence of one or two bright galaxies, neither can they be explained by completeness issues. This was confirmed by a simple test performed on the SDSS sample, in which we constructed an alternative completeness function on the basis that *all* the galaxies detected within the virial radius were considered group members unless specifically excluded by the spectroscopy. This clearly produces a gross overestimate of the total luminosities of these groups. Nevertheless, the increase in luminosity found of ∼0.25 dex does not qualitatively change our conclusion that fossils exhibit mass-to-light ratios greater than those of normal systems of the same mass. This can most easily be seen by considering Fig. 4 as the reduction in log[M/L] of 0.25 dex, which is of the same magnitude as the plotted errors; this does not change the conclusion that the fossils lie in the outer envelope of data for normal systems. The high mass-to-light ratios that we find in fossil systems are therefore robust to completeness and calibration issues.

We next consider the optical properties of the sample in more detail in order to better characterize these systems.

5.4 Optical properties

In this section we look in detail at the optical properties of our fossil systems (luminosities, LFs and m_{12} gaps). The data are presented in Table 3.

5.4.1 The m_{12} gaps

The estimated values of m_{12} are presented in Table 3. Two sets of values are given, one ($m_{12,S}$) is measured within the radius used in the selection process ($R_{200,S}$), the other ($m_{12,X}$) is measured within $R_{200,X}$. Now, we demonstrated in Section 3.1 that for our samples $R_{200,X}$ is typically ∼50 per cent larger than $R_{200,S}$. It can be seen from Table 3 that this results in significant reductions in the observed m_{12} in many cases, with only 3/10 *strictly* meeting the Jones et al. (2003) criterion of a 2-mag gap within $0.5R_{200}$.

As previously noted (Section 3.1), in the RXJ sample, the disparity between $R_{200,S}$ and $R_{200,X}$ is caused by the difference in X-ray properties derived from the *ROSAT* data reported in Jones et al. (2003) and the higher quality *Chandra* data reported in KPJ07 (and used in this work).

In the SDSS sample, we find that the discrepancy can be explained by the high mass-to-light ratios found in these groups. Recall that Johnston et al. (2007) binned the maxBCG systems by optical richness in order to carry out the weak lensing analysis from which the $R_{200,S}$ values were derived. This implicitly assumes that all systems of the same richness have the same mass (and hence the same R_{200}). Now, given that we find the systems in our sample of FGs to have high mass for their luminosity (and richness), it follows that the values of R_{200} derived for these systems by the Johnston et al. (2007) analysis will be underestimated.

Clearly, these issues have a significant effect on the values of m_{12} derived for our samples. However, this problem is not confined to the two samples considered in our paper. Indeed, in *most* studies in

the literature the definition of fossil groups proposed in Jones et al. (2003) – i.e. a 2-mag gap within half the virial radius – is not strictly followed. For instance, in some studies (e.g. Santos, Mendes del Oliveira & Sodré 2007; Smith et al. 2010) a fixed radius of 0.5 Mpc is used (in systems many of which have properties suggesting viral radii greater than 1.0 Mpc). In other studies (e.g. La Barbera et al. 2009; Voevodkin et al. 2010; Aguerri et al. 2011) both a radius less than $0.5R_{200}$ *and* a reduced m_{12} gap were employed as the definition of FGs. In those studies that *do* strictly apply the Jones et al. (2003) criteria (e.g. Zibetti, Pierini & Pratt 2009; Démoclès et al. 2010; Lopes de Oliveira et al. 2010 and our study), a significant fraction ($\geq$50 per cent) of systems previously identified as FGs fail to meet the criteria. In fact, recent works (Santos et al. 2007; Zibetti et al. 2009; our study) have shown that even the Jones et al. (2003) study, in which the FG criteria were defined, underestimated the virial radius of many of the systems it reports, and therefore *also* used a radius less then $0.5R_{200}$. This is, most poignantly, found to be true for the *prototypical* system identified in Ponman et al. (1994) (i.e. RXJ1340), which fails a strict application of the Jones et al. (2003) criteria.

We are therefore left with the choice of either discarding more than 50 per cent of the FG data in the literature (including the prototypical system; RXJ1340) or allowing a relaxation of the selection criteria. Such a relaxation amounts to simply accepting that the systems under discussion represent the most extreme cases of large magnitude gaps identified to date. Since, as noted in many of the above papers, the original criteria are somewhat arbitrary, we have elected to take the same approach as that in the majority of literature studies and relax the FG criteria. We therefore simply note that eight out of 10 of the groups in our sample meet a definition of fossil groups as systems with $m_{12} > 2.0$ mag within $0.5R_{200,\mathrm{S}}$ (which corresponds to $\sim 0.33R_{200,\mathrm{X}}$), while the two systems that fail these criteria still exhibit large gaps within this radius.

Next, let us consider the $m_{12,S}$–L_{bcg} data from the maxBCG catalogue. These are presented in Fig. 5 (NB: these data are also reported, in a slightly different form, in Miller et al. 2011). In this figure, the diagonal lines mark the loci of the second-ranked galaxies of constant luminosity. Individual data points are coloured by richness (blue for $N_{200} < 25$, red for $N_{200} > 25$; see Miller et al. 2011, for the definition of richness). The groups detailed in this work are identified by circles (the SDSS sample) and squares (the RXJ sample). There are a total of 1128 systems shown in this plot. It may be noted that these data were taken directly from the maxBCG catalogue. The BCG luminosities are therefore not scaled to the cosmology generally used in this paper.

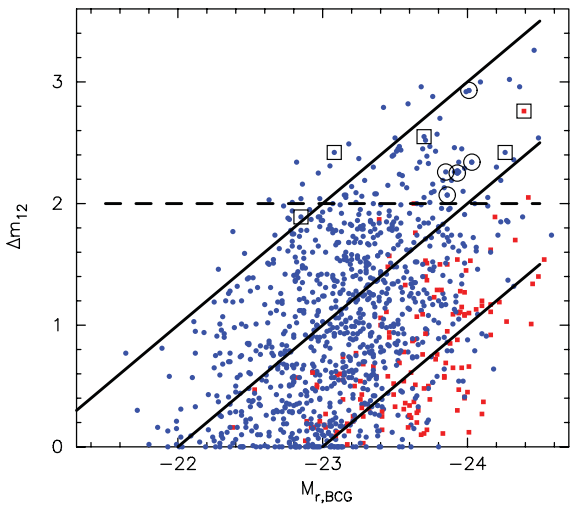

Figure 5. Luminosity gap ($m_{12,\mathrm{S}}$) is plotted against BCG absolute magnitude. The lines of constant second-ranked galaxy luminosity are marked by (diagonal) lines. These correspond to (from top to bottom) $M_2 = -21, -22$ and -23 mag. Systems reported in this work are identified by circles (the SDSS sample) and squares (the RXJ sample). Points are coloured to indicate richness, with low-richness groups ($N_{200} \leq 25$) in blue and high-richness groups ($N_{200} > 25$) in red.

An examination of Fig. 5 reveals three important properties of all systems exhibiting $m_{12} > 2$ mag (i.e. not just those analysed in this work) as follows.

(i) Most of the BCGs in these systems are extremely bright. Indeed, many are amongst the brightest in the whole sample, and very few systems exhibit $M_{r,\mathrm{BCG}} > -23$ mag.

(ii) Most of these systems possess very low luminosity second-ranked galaxies, with very few systems exhibiting $M_{r,2} \leq -22$ mag.

(iii) Nearly all systems with $m_{12} > 2$ mag exhibit low richness. Indeed, the average richness of all the 93 systems with $m_{12} > 2$ mag is only 13.0. Only two systems with $m_{12} \geq 2$ mag exhibit $N_{200} > 25$. These include J1416 (a member of our sample), which has $N_{200} = 28$, and another system with $N_{200} = 48$.

It is interesting to note that the last of these results implies that the low-richness criterion applied in the selection of the SDSS sample (Section 2.1) was largely redundant. It should also be noted that the high luminosities of the BCGs in our samples are highly selection biased, as the SDSS sample was *specifically* selected to contain only systems with bright BCGs (see Section 2.1), whereas the RXJ sample was biased towards high-luminosity BCGs by the selection of systems with low ratios of X-ray to BCG optical luminosity (in systems already known to be bright in the X-ray), as well as the selection of '. . . . . system[s] dominated by a single galaxy' (Jones et al. 2003). However, this selection criterion too is largely redundant, as the simple selection of samples with $m_{12} > 2$ mag automatically ensures a significant population of bright BCGs.

Now, the finding above – that FGs are found in systems with bright BCGs and low-luminosity second-ranked galaxies – is perhaps not surprising. However, the realization that these high-mass systems, with appropriately bright BCGs, are low-richness systems points to a new interpretation of these objects.

An important consideration in this new interpretation of fossil systems is that there is a causal link between points (ii) and (iii) above. Namely, that low-richness systems are *expected*, on average, to have low-luminosity second-rank galaxies, simply due to the effect of sparse sampling of the Schechter function. This effect is clearly demonstrated in the bottom panel of fig. 10 of Hansen et al. (2005), in which the number of bright galaxies present in the systems declined rapidly as richness decreased from moderate to low values. To further develop this point, in the next section we present a completeness-corrected, composite LF for the five systems in the SDSS sample (which, unlike the RXJ sample, have a high completeness out to the virial radius).

5.5 The luminosity function

The results of our analysis of the group LFs of the SDSS sample in each of the *g*, *r* and *i* bands are shown in Fig. 6.

This analysis is limited by the completeness limit of the SDSS photometry of about $\sim$21 mag in the *r* band. For the composite LF, we assume the limit to the absolute magnitude to be -18 for the *g* band, and -18.5 for the *r* and *i* band. These conservative limits

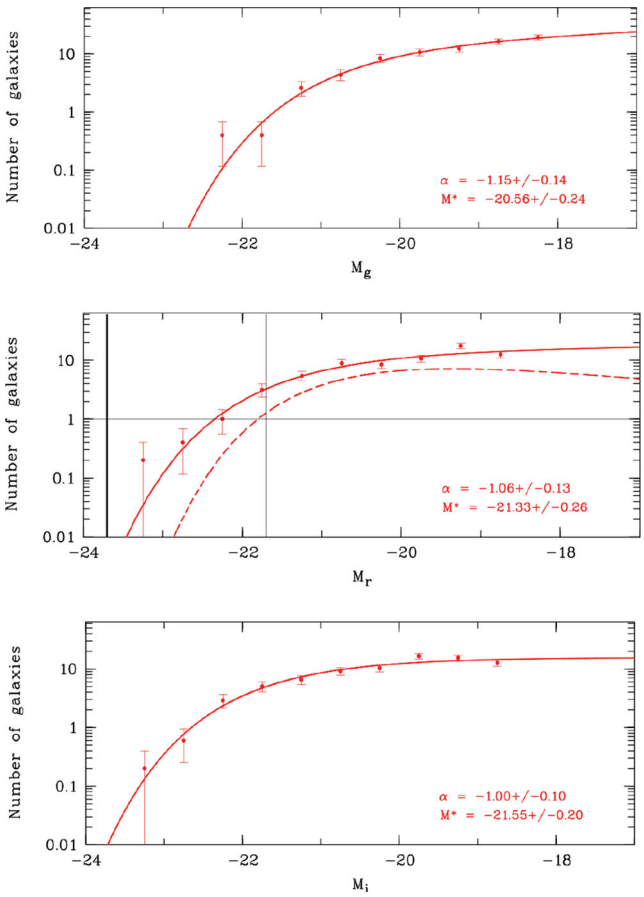

Figure 6. Composite luminosity function for five fossil group candidates, J0906, J1045, J0856, J1136 and J1017. The solid red line is the composite (average) luminosity function within $R_{200,X}$ for all the five systems. The dashed line in the *r*-band plot is the composite (average) luminosity function within $0.5R_{200,X}$. The dark vertical line in the *r*-band plot marks the average BCG luminosity, while the faint line marks the point 2 mag fainter.

were set to make sure that the individual LFs were considered inside reasonable completeness limits, before including them in the composite LFs. All galaxies meeting these limits and within $R_{200,X}$ of each system were included, and the LF averaged. The number of galaxies (*y*-axis of Fig. 6) therefore represents the number of galaxies per magnitude found within $R_{200,X}$ of a single, average group.

The best fit for α and M^* for the three bands are -1.15 and -20.56 mag for *g*, -1.06 and -21.33 mag for *r* and -1.00 and -21.55 mag for *i*. The derived LFs are shown in Fig. 6 as solid red lines. Also shown in the *r*-band plot is the LF within $0.5R_{200,X}$) which exhibits α and M^* of -0.69 and -20.62. The error bars on our derived LFs are large, due to the relatively small number of galaxies used in their construction. The results are therefore consistent with a broad range of literature studies. We do, however, note a particularly good agreement between the α and M^* values that we derive in the *r* band within $R_{200,X}$ and the values of Blanton et al. (2003) for ∼150 000 galaxies in the SDSS spectroscopic survey.

It should be remembered that the LFs presented in Fig. 6 are the *average* of five individual groups. The *y*-axis of Fig. 6 therefore represents the expected number of galaxies per magnitude bin of a single, average group.

Now, we are concerned with describing the $m_{12,S}$ gaps which are defined to be within $0.5R_{200}$. Our analysis therefore proceeds by considering the *r*-band LF within $0.5R_{200,X}$ (Fig. 6, middle plot, dashed line). It is evident from this plot that the expected number of galaxies per magnitude is below 1.0 *over the entire 2-mag range immediately below the luminosity of the BCG*. This clearly indicates that m_{12} gaps are likely to be large in such low-richness, bright BCG systems. The effect can be quantified by integrating along the LF over this 2-mag range. The derived value of 0.4 indicates that ∼60 per cent of all such systems will possess *no* galaxies within this magnitude range (and therefore possessing $m_{121,S} > 2.0$ mag). Analysis of the data shown in Fig. 5 shows that, in fact 50 per cent of the 62 low-richness ($N_{200} < 25$) systems with bright BCGs ($M_{r,bcg} < -23.5$ mag) possess $m_{121,S} > 2.0$ mag, in a reasonably good agreement with our estimate from the *r*-band LF of 60 per cent.

This result is in sharp contrast with Jones et al. (2003) who performed Monte Carlo simulations using the LF of MKW/AWM clusters from Yagamata & Maehara (1986), finding an extremely low incidence of systems with $m_{12} > 2.0$ mag. However, it is not clear from their paper what value of BCG luminosity was used. We therefore performed our analysis again, this time using the Yagamata & Maehara values for M^*, α and BCG luminosity (-21.57, -1.07 and -23.0 mag, respectively). Our analysis indicates that using these values the expectation of the number of galaxies within 2 mag of the BCG is 3.4. We therefore confirm that such an analysis results in extremely low probabilities of finding fossil groups. Indeed, assuming simple Poisson statistics, the average of 3.4 galaxies within 2 mag of the BCG would suggest fossil systems with $m_{12} > 2.0$ mag to be 2σ events, consistent with the low numbers reported in Jones et al. (2003).

The cause of the disparity between the Jones et al. results and ours is therefore likely to be due to the difference in the gaps between M^* and L_{bcg} in the two studies, i.e. 2.5 mag in our study, but only 1.5 mag in the Yagamata & Maehara (1986). We therefore conclude it to be likely that the Jones et al. (2003) analysis did not consider the extremely bright BCGs found in fossil systems.

In summary, our analysis shows that large m_{12} gaps are an expected feature in low-richness systems that host bright BCGs, and that this effect alone can account for the properties of the fossil systems in our study, without taking recourse to additional processes such as dynamical friction.

5.6 Synthesis

In this section we draw together the various strands of our analysis in order to gain a clearer insight into the nature of the fossil systems that we have investigated, and to identify outstanding issues.

First, let us recall the two most important conclusions of our analysis of the scaling relations of fossil system. Namely, that these systems possess high masses and, despite the high luminosities of their BCGs, they have low *total* optical luminosities (Section 5.3).

Considering the bright BCG luminosities and high system masses, it can be seen from the plot of BCG luminosity against mass ($M_{200,dyn}$) in Hansen et al. (2009; their fig. 13) that the values found for our fossil groups (average $L_{bcg} = 2.3 \times 10^{11}$ L$_\odot$, $M_{200} = 2.3 \times 10^{14}$ M$_\odot$) are consistent with values found for normal systems in the SDSS. Indeed, fig. 13 of Hansen et al. (2009) indicates that, for a mass of 2.3×10^{14} M$_\odot$, a typical BCG luminosity is 2×10^{11} L$_\odot$ (after the Hansen et al. data are *k*-corrected to $z = 0$ and adjusted to the cosmology used in this work). In other words, the BCG luminosities in these fossil systems are entirely consistent with their masses, but are inconsistent with either their richnesses or total optical luminosities.

The difference between fossils and normal systems can also be seen by examining the plot of the fraction of optical light in the BCG ($f_{\rm bcg}$ in our Table 3) against the M_{200} of SDSS groups and clusters as shown in the top panel of fig. 14 of Hansen et al. (2009). For masses appropriate for our sample, this plot shows that normal systems with masses appropriate for our fossil sample (2.3×10^{14} M$_\odot$) possess $f_{\rm bcg} \approx 0.1$ (again after the Hansen et al. data are adjusted to the cosmology used in this work). Comparison of this value to the value of $\sim$0.3 found in fossil systems therefore again suggests a factor of $\sim$3 underluminosity in fossils systems compared to normal systems, consistent with the value found by consideration of the L_r–σ plot (Fig. 3 and Section 5.3).

Now, given that we find the luminosities of the BCGs to be comparable between fossil and normal samples of the same mass, the discrepancy in the optical luminosity must be due to a significant underabundance of *non*-BCG galaxies. Indeed, simple arithmetic shows that, if the whole deficit is due to the lack of non-BCG galaxies, then, in order that the *total* luminosity be $\sim$3 times lower than normal systems, fossil must contain only $\sim$25 per cent of the non-BCG galaxies found in a normal cluster of the same mass.

5.7 The role of dynamical friction

Given our results it is interesting to look at the possible role of dynamical friction in generating the large m_{12} gaps in our fossil sample. Our considerations are based on the LF derived for the average of the five groups in the SDSS sample, as detailed above.

Consider the *r*-band LFs in Fig. 6. If we assume that dynamical friction has caused even a single bright galaxy to be 'cannibalized' by the central BCG of each group, then replacing this galaxy in the LF within R_{200} (i.e considering what this LF looked like *before* dynamical friction has had its effect) results in an LF that shows a significant excess of bright galaxies with respect to any reasonable Schechter function, i.e. there would be as many, or *more*, galaxies with luminosity ~-23 mag than there galaxies with luminosity ~-22 mag. The problem is even more pronounced if the putative cannibalized galaxies are replaced in the LF within $0.5R_{200}$ (dashed line in the middle panel of Fig. 6).

Therefore, while our data do not address the role of dynamical friction in the building of the LF and BCG at early times, the data do suggest that, if dynamical friction *has* played a part in generating the large m_{12} gaps and bright BCGs at later times, then our sample of fossil groups must have started with abnormal LFs.

6 DISCUSSION

The picture painted by our analysis can then be summarized as follows: fossil groups differ significantly from non-fossils systems of the same mass *only* in that fossil groups exhibit a large underabundance of non-BCG galaxies. We note that this description is highly efficient in that it simultaneously describes the similarities and differences between fossil and normal systems for a host of observables (e.g. N_{200}, m_{12}, $L_{\rm bcg}$, $L_{\rm tot}$, $L_{\rm X}$, $T_{\rm X}$ and σ).

In the light of these conclusions, a number questions (but, unfortunately, not many answers) immediately present themselves.

(1) *Where are all the missing bright baryons?*
There are three immediately apparent ways to account for the 'missing' baryons as follows.

(i) They have been expelled from the system (although it is difficult to see how this could be accomplished without a significant loss of X-ray emitting gas, which has not been detected).

(ii) They are 'hidden', possibly locked up in the hot X-ray gas or the warm/hot intergalactic medium, suggesting a low galaxy formation efficiency. Alternatively, they could be 'hidden' from our luminosity budget as intracluster light (although this seems unlikely, as the high velocity dispersions and low galaxy number densities exhibited by the groups in our sample suggest the interactions that generate intracluster light would be rare and weak).

(iii) They were never present, not at all, with the systems forming in regions of space deficient in baryons (although it is difficult to see how the bright BCGs could have formed in such circumstances).

(2) Are fossils really fossils? That is, are they truly *old*?
It is difficult to see how such low mass-to-light ratio systems could have formed *recently*. Significant merger/accretion activity might also be ruled out as this would have both ameliorated the high mass-to-light ratios and provided a significant source on non-BCG galaxies (the one thing above all else that these systems lack). It therefore seems safer to conclude that these are indeed ancient systems, and that they are indeed worthy of the title *fossil* groups.

(3) What do our results mean for studies that utilize cosmological *N*-body/semi-analytic modelling to address issues surrounding fossil groups?
As far as the authors are aware, no such study to date has identified fossils as being associated with low richness systems. Whether this is a failure of the studies themselves or rather represents a failure in the baryonic physics in the semi-analytical models used in the cosmological simulations remains to be seen.

(4) By what mechanism could the BCGs in the low-richness systems of fossil groups achieve the same mass as those in much richer systems?
Our results appear to present a challenge to the currently accepted paradigm of BCG formation through hierarchical clustering within the host halo (e.g. de Lucia & Blaizot 2007), since the massive (luminous) BCGs found in our sample of fossil systems appear to have formed in extremely low galaxy number-density environments, and should therefore have been relatively starved of the raw material necessary for such a hierarchical assembly path.

All of these issues clearly need to be addressed in the near future if we are to establish a coherent picture of how the formation of fossil systems differs from normal systems.

7 CONCLUSIONS

We present a kinematic analysis of 10 fossil group candidates, five of which have been previously identified as fossil groups in the literature. The other five candidates investigated were optically selected from the maxBCG catalogue of Koester et al. (2007), spectroscopically observed with the Magellan IMACS instrument and followed up with *Chandra* X-ray snapshot observations. For these 10 groups, between 10 and 64 galaxies (with an average of $\sim$33) are confirmed as group members within $R_{200,\rm X}$. This study therefore represents the deepest study of a significant number of fossil systems to date.

We confirm previous findings that the majority of the FGs identified to date lie in the regions of X-ray luminosity, X-ray temperature and velocity dispersion scaling relations occupied by galaxy *clusters* rather than groups. Since all three of these parameters ($L_{\rm X}$, $T_{\rm X}$ and σ) can be used as proxies for mass, and all three yield masses consistent with cluster masses ($\sim10^{14}$ M$_\odot$, or greater), we can be confident of these mass estimates. We find that the luminosities of the brightest cluster galaxies in our sample are also consistent with these high masses, lending further support to this finding.

However, there is one parameter that is *not* consistent with cluster values – namely the total optical luminosities of these systems. We find that the fossil groups in our sample are, on average, underluminous by a factor of ∼3 with respect to galaxy clusters of the same mass. High mass-to-light ratios have been noted in previous works (e.g. Jones et al. 2003; Yoshioka et al. 2004; Cypriano et al. 2006; Mendes de Oliveira et al. 2006; KPJ07), but no firm conclusions were drawn from these relatively small samples. Here, however, we find this to be essentially the defining feature of fossil systems, showing that these systems are characterized by their possession of only ∼25 per cent of the non-BCG galaxies found in normal systems of the same mass. We show that this low richness can simultaneously account for the large m_{12} gaps *and* the high mass-to-light ratios.

We note that *none* of the paradigms for the formation of fossils (and particularly the paradigm of cannibalism of bright central galaxies by the BCG) predicts such high masses coupled with low luminosities. Our findings therefore suggest that a new paradigm for the formation and evolution of fossil groups is required.

ACKNOWLEDGMENTS

This work is based on observations made with the 6.5-m Magellan/Baade telescope, a collaboration between the Observatories of the Carnegie Institution of Washington, University of Arizona, Harvard University, University of Michigan and Massachusetts Institute of Technology, and at the Cerro Tololo Inter-American Observatory, a division of the National Optical Astronomy Observatories, which is operated by the Association of Universities for Research in Astronomy, Inc., under a cooperative agreement with the National Science Foundation. The COSMOS pipeline supplied by the Magellan consortium was used for data reductions. This research also made use of NASA's Astrophysics Data System, as well as the IRAF and STARLINK software. IRAF is distributed by the National Optical Astronomy Observatories, which is operated by the Association of Universities for Research in Astronomy, Inc. (AURA) under a cooperative agreement with the National Science Foundation. Also presented are observations obtained at the Gemini Observatory, which is operated by the Association of Universities for Research in Astronomy, Inc., under a cooperative agreement with the NSF on behalf of the Gemini partnership: the National Science Foundation (United States), the Science and Technology Facilities Council (United Kingdom), the National Research Council (Canada), CONICYT (Chile), the Australian Research Council (Australia), Ministério da Ciência e Tecnologia (Brazil) and Ministerio de Ciencia, Tecnología e Innovación Productiva (Argentina). RD acknowledges support from NASA Grant NNH10CD19C and partial support from Chandra Award No. GO9-0142A. RLO acknowledges financial support from the Brazilian agency FAPESP (Fundação de Amparo à Pesquisa do Estado do São Paulo) through a Young Investigator Program (numbers 2009/06295-7 and 2010/08341-3). RNP also acknowledges financial support from the Brazilian agency FAPESP (programme number 2008/57331-0). ESC also acknowledges support from FAPESP (programme number 2009/07154-8-0) and CNPq.

REFERENCES

Aguerri J. A. L. et al., 2011, A&A, 527, 143
Bauer A. E., Grützbauch R., Jørgensen I., Varela J., Bergmann M., 2011, MNRAS, 411, 2009
Becker M. R. et al., 2007, ApJ, 669, 905
Beers T. C., Flynn K., Gebhardt K., 1990, AJ, 100, 32
Bertin E., Arnouts S., 1996, A&AS, 117, 393
Blanton M. R. et al., 2003, AJ, 592, 819
Carlberg R. G. et al., 1997, ApJ, 485, L13
Cypriano E. S., Mendes de Oliveira C. L., Sodré L., Jr, 2006, AJ, 132, 514
D'Onghia E., Sommer-Larsen J., Romeo A. D., Burkert A., Pedersen K., Portinari L., Rasmussen J., 2005, ApJ, 630, L109
Dariush A. A., Khosroshahi H. G., Ponman T. J., Pearce F., Raychaudhury S., Hartley W., 2007, MNRAS, 382, 433
de Lucia G., Blaizot J., 2007, MNRAS, 375, 2
Démoclès J., Pratt G. W., Pierini D., Arnaud M., Zibetti S., D'Onghia E., 2010, A&A, 517, 52
Fujita Y., 2004, PASJ, 56, 29
Girardi M., Giuricin G., Mardirossian F., Mezzetti M., Boschin W., 1998, ApJ, 505, 74
Girardi M., Manzato P., Mezzetti M., Giuricin G., Limboz F., 2002, ApJ, 569, 720
Gunn J. E., Gott J. R., 1972, ApJ, 176, 1
Hansen S. M., McKay T. A., Wechsler R. H., Annis J., Sheldon E. S., Kimball A., 2005, ApJ, 633, 122
Hansen S. M., Sheldon E. S., Wechsler R. H., Koester B. P., 2009, ApJ, 699, 1333
Helsdon S. F., Ponman T. J., 2003, MNRAS, 340, 485
Hilton M. et al., 2010, ApJ, 718, 133
Johnston D. E. et al., 2007, preprint (arXiv:0709.1159)
Jones L. R., Ponman T. J., Horton A., Babul A., Ebeling H., Burke D. J., 2003, MNRAS, 343, 627
Kawata D., Mulchaey J. S., 2008, ApJ, 672, L103
Khosroshahi H. G., Maughan B. J., Ponman T. J., Jones L. R., 2006, MNRAS, 369, 1211
Khosroshahi H. G., Ponman T. J., Jones L. R., 2007, MNRAS, 377, 595 (KPJ07)
Koester B. P. et al., 2007, ApJ, 660, 239
La Barbera F., de Carvalho R. R., de la Rosa I. G., Sorrentino G., Gal R. R., Kohl-Moreira J. L., 2009, AJ, 137, 3942
Landolt A. U., 1992, AJ, 104, 340
Lopes de Oliveira R., Carrasco E. R., Mendes de Oliveira C., Bortoletto D. R., Cypriano E., Sodr L., Jr, Lima Neto G. B., 2010, AJ, 139, 216
Maurogordato S., Sauvageot J. L., Bourdin H., Cappi A., Benoist C., Ferrari C., Mars G., Houairi K., 2010, preprint (astro-ph:1009.1967)
Mendes de Oliveira C. L., Cypriano E. S., Sodré L., Jr, 2006, AJ, 131, 158
Mendes de Oliveira C. L., Cypriano E. S., Dupke R. A., Sodré L., Jr, 2009, AJ, 138, 502
Miller E. D. et al., 2011, MNRAS, preprint (arXiv:1109.4167)
Navarro J. F., Frenk C. S., White S. D., 1995, MNRAS, 275, 720
Osmond J. P. F., Ponman T. J., 2004, MNRAS, 350, 1511
Ponman T. J., Allan D. J., Jones L. R., Merrifield M., McHardy I. M., Lehto H. J., Luppino G. A., 1994, Nat, 369, 462
Ramella M., Boschin W., Geller M. J., Mahdavi A., Rines K., 2004, AJ, 128, 2022
Rasmussen J., Ponman T. J., Mulchaey J. S., 2006, MNRAS, 370, 453
Rozo E. et al., 2009, ApJ, 703, 601
Rykoff E. S. et al., 2008, MNRAS, 387, L28
Santos W. A., Mendes de Oliveira C., Sodré L., Jr, 2007, AJ, 134, 1551
Schechter P., 1976, ApJ, 203, 297
Sheldon E. S. et al., 2009, ApJ, 703, 2217
Smith G. P. et al., 2010, MNRAS, 409, 169
Strazzullo V. et al., 2010, A&A, 524, 17
Vikhlinin A., McNamara B. R., Hornstrup A., Quintana H., Forman W., Jones C., Way M., 1999, ApJ, 520, L1
Voevodkin A., Borozdin K., Heitmann K., Habib S., Vikhlinin A., Meschcryakov A., Hornstrup A., Burenin R., 2010, ApJ, 708, 1376
Wu X.-P., Xue Y.-J., Fang L.-Z., 1999, ApJ, 524, 22
Yagamata T., Maehara H., 1986, PASJ, 38, 661

Yoshioka T., Furuzawa A., Takahashi S., Tawara Y., Sato S., Yamashita K., Kumai Y., 2004, Advances Space Res., 34, 2525
Zhang Y.-Y., Andernach H., Caretta C. A., Reiprich T. H., Böhringer H., Puchwein E., Sijacki D., Girardi M., 2011, A&A, 526, 105
Zibetti S., Pierini D., Pratt G. W., 2009, MNRAS, 392, 525

APPENDIX A: THE EFFECTS OF SUBSTRUCTURE

In this appendix we detail our analysis of the uncertainty in our derived velocity dispersions in the three systems in our study that possess the strongest indications of the presence of substructure (J1017, J1256 and J1416, as described in Section 5.1).

Fig. A1 shows the spatial distribution of member galaxies of these three groups. Circles representing $R_{200,X}$ are shown. Unfortunately, even with the increase in the numbers of spectroscopically confirmed members compared to previous studies, the incomplete spatial coverage of our data results in it still being insufficient for a full 'friends-of-friends' type of analysis. Here, we therefore simply test the likely impact of potential substructures on our derived parameters in the three systems including them in, or excluding them from, our analysis.

A0.1 J1017

In the case of J1017, there are a significant number of galaxies with high recession velocities ($>900\,\mathrm{km\,s^{-1}}$) located just outside $R_{200,X}$. An examination of Fig. A1 shows them to be located to the north-east and south and south-west of the group in a configuration which suggests that these galaxies are unlikely to be group members under the assumption that the group is virialized. However, to test for the impact of including these galaxies in our kinematic measurements, we recalculated the velocity dispersion and ΔRV_{BCG} including these galaxies. The effect was to increase the measured velocity dispersion from 474 ± 71 to $643 \pm 88\,\mathrm{km\,s^{-1}}$ (an increase in $\log\sigma$ of 0.13 dex). Comparison of the dynamical R_{200} (as defined in the previous section and given in Table 2) with the X-ray derived value (Table 1) shows an almost perfect agreement. Therefore, the dynamical R_{200} that would be derived from the increased value of velocity dispersion when the outlying galaxies are included would exceed the X-ray derived value by nearly 40 per cent. Their inclusion also results in a significant decrease in ΔRV_{BCG}, with the value going from $+73 \pm 101$ to $-129 \pm 125\,\mathrm{km\,s^{-1}}$. Therefore, while we can draw no firm conclusions, the data suggest that these high-radius, high recession velocity galaxies are not part of the virialized system.

A0.2 J1256

For J1256 we see an apparent excess of low recession velocity galaxies (Fig. 2). An examination of Fig. A1 shows that these galaxies all lie on one side of the group. Indeed, the group is remarkably reminiscent of the 'bimodal' clusters reported in Maurogordato et al. (2010). The BCG also exhibits a large positive recession velocity with respect to the group average of (ΔRV_{BCG}, Table 2). We therefore again recalculated the velocity dispersion and dynamical R_{200}, this time excluding galaxies with absolute recession velocities less than $-800\,\mathrm{km\,s^{-1}}$. This resulted in a velocity dispersion of $449 \pm 70\,\mathrm{km\,s^{-1}}$ and a ΔRV_{BCG} of $-115 \pm 100\,\mathrm{km\,s^{-1}}$. The reduction in velocity dispersion of 28 per cent (0.14 dex in $\log\sigma$) results in a reduction in the dynamical R_{200} such that it becomes 20 per cent lower than the X-ray derived value rather than the 16 per cent overestimate of the value given in Table 2. We are therefore unable to definitively state whether these objects are part of the virialized structure on the basis of the velocity dispersion measurements. In addition, while the large positive ΔRV_{BCG} is eliminated, its replacement by the relatively large negative value means that no firm conclusions can be drawn from this parameter either. However, examination of the X-ray contours (Fig. A2) of this group indicates no obvious sign

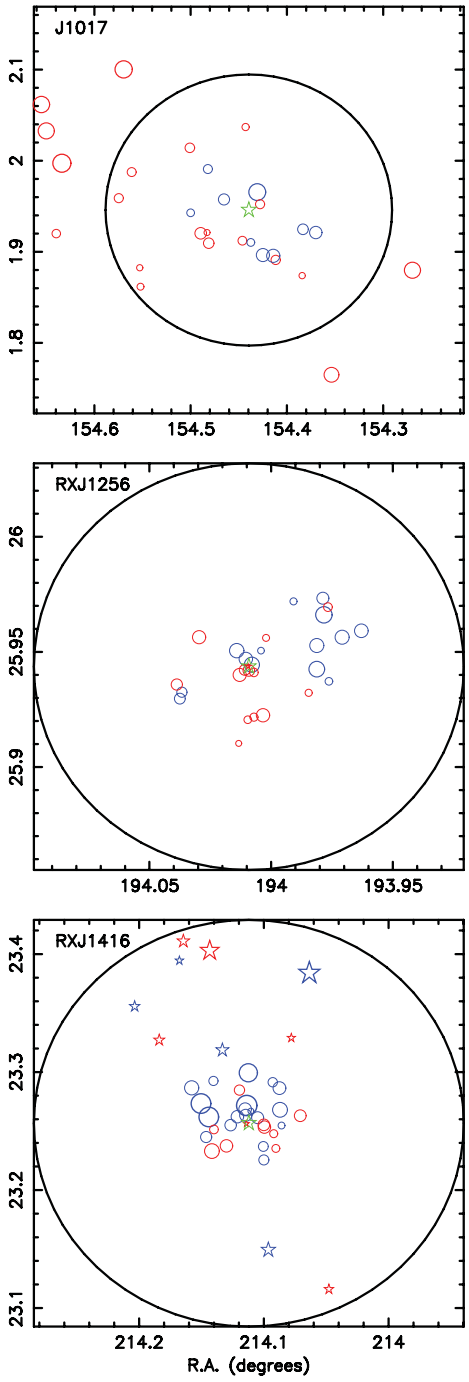

Figure A1. The spatial distributions of galaxies with recession velocities within $2000\,\mathrm{km\,s^{-1}}$ of the BCG (green star) are shown. The symbol colour indicates the *sense* of the recession velocity with respect to the BCG (red for redshift, blue for blueshift). Symbol size denotes the *magnitude* of the recession velocity with large symbols representing greater absolute velocities. Stars identify galaxies whose recession velocities were taken from the SDSS spectroscopic catalogue. Solid circles mark the $R_{200,X}$ radius.

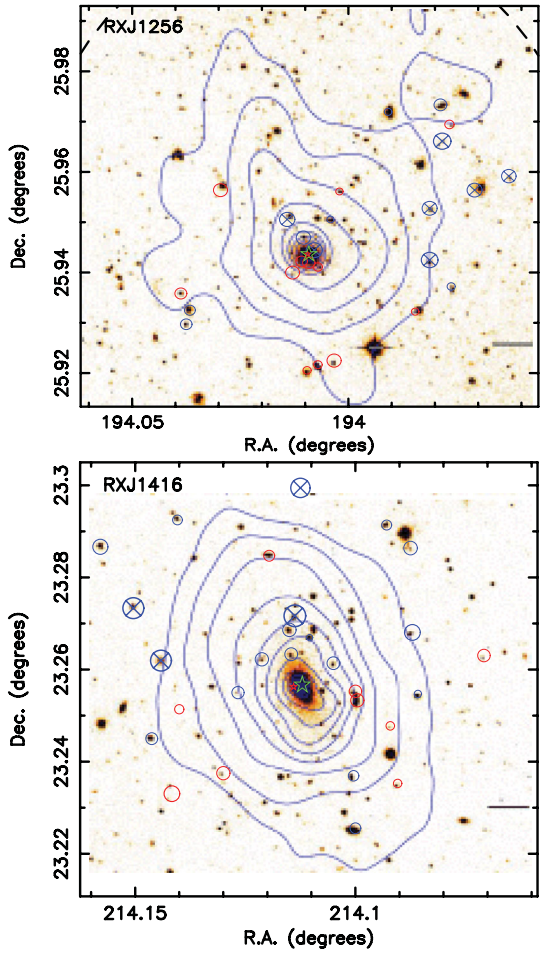

Figure A2. Our recession velocity data for J1256 and J1416 are overlayed on *Chandra* X-ray contours from KPJ07.

of substructure associated with the overall projected location of the highly blueshifted galaxies. In fact, the X-ray isophotes seem to show an elongated substructure towards the N-NE, consistent with some dynamical turmoil, so that the subsystem of velocity outliers may be the results of the previous interaction with another group and the system may not be fully virialized. A more complete study of this group is necessary to confirm these findings.

We also note that a close examination of the central galaxy of this system reveals two extremely nearby (on the plane of the sky), relatively bright galaxies that have not to date been examined spectroscopically (either by us or the SDSS), and whose membership therefore remains untested. The brighter of these two galaxies is only 1.83 mag fainter in the r band than the central galaxy.

A0.3 J1416

In J1416 we see a substantial collection of low recession velocity galaxies in Fig. 2 which are separated in redshift space from the remainder of the group by a significant gap. An examination of Fig. A1, once again, shows that all the low-z galaxies lie on one side of the group, again reminiscent of the bimodal clusters reported in Maurogordato et al. (2010). The group also exhibits the largest $\Delta RV_{\rm BCG}$ in our sample. We therefore recalculated the velocity dispersion and dynamical R_{200}, this time excluding galaxies with absolute recession velocities less than $-1400\,{\rm km\,s^{-1}}$. Once again, we find the large $\Delta RV_{\rm BCG}$ to be eliminated (becoming $+74 \pm 98\,{\rm km\,s^{-1}}$), and the velocity dispersion to be reduced to $560 \pm 68\,{\rm km\,s^{-1}}$ (a reduction of 0.16 dex in $\log\sigma$). The dynamical R_{200} is therefore reduced from 16 per cent greater than the X-ray derived value to 15 per cent lesser – again inconclusive. However, in this case, the X-ray profile also exhibits signs of disturbance in the sense that it is extended along the same axis as the kinematic substructure (Fig. A2). On balance the data therefore suggest that this group is subject to an going interaction/merger.

Evidence for merging is also present in the X-ray spectral analysis. J1416 is the hottest and most luminous fossil group known, with gas temperatures reaching 4 keV! It has, at larger scales, a temperature decline seen with *XMM–Newton*. As shown by Khosroshahi et al. (2006), this unusual fossil group has a temperature 'spike' of $\sim$200 kpc from the centre, followed by a strong temperature decline at $r > 200$ kpc. The spike could be due to azimuthal temperature substructures in the intergalactic medium. The cooling time of 5 Gyr measured for this system is significantly below the Hubble time for regions with the central 150 kpc (Khosroshahi et al. 2006), but the expected level of cooling is not observed, implying that some extra source of gas heating is in effect, maybe shock heating due to merging.

APPENDIX B: DATA

In this appendix we present the recession velocity and apparent magnitudes for systems with new data reported in this paper (SDSS J0906+0301, SDSS J1045+0420, SDSS J1136+0713, SDSS J0856+0553, SDSS J1017+0156, RX J1256.0+2556 and RX J1331.5+1108). For the corresponding data for groups taken from the literature (RX J1340.5+4017 RX J1416.4+2315 and RX J1552.2+2013), see Mendes de Oliveira et al. (2009), Cypriano et al. (2006) and Mendes de Oliveira et al. (2006), respectively. In each group the first galaxy (with zero recession velocity) is the BCG and the source of the spectroscopic data used to derive recession velocities is identified (i.e. Magellan, Gemini or the SDSS data base).

Table B1. SDSS J0906+0301.

RA	Dec.	*RV*	*g*	*r*	*i*
Magellan data					
09:06:38.27	03:01:39.1	0	16.67	15.54	15.09
09:06:54.70	03:02:29.7	545	18.22	17.13	16.66
09:06:50.68	03:00:02.4	−7	18.34	17.29	16.86
09:06:33.72	03:02:00.9	74	19.73	18.63	18.18
09:06:30.98	03:01:35.3	−275	19.74	18.74	18.29
09:06:39.36	03:00:44.7	−246	19.78	18.76	18.28
09:06:46.50	02:59:21.8	940	19.52	18.87	18.52
09:06:43.25	03:02:06.0	−211	20.19	19.18	18.70
09:06:46.05	03:03:17.6	167	20.23	19.25	18.75
09:06:34.81	02:59:45.2	1120	20.23	19.43	18.95
09:06:34.13	03:03:33.8	−224	20.71	19.75	19.42
09:06:39.59	03:01:34.2	213	20.00	19.81	20.56
09:06:29.70	03:01:03.4	−909	20.93	19.89	19.56
09:06:48.28	03:06:09.4	342	19.21	18.11	17.67
09:06:50.07	03:03:41.5	−297	19.41	18.35	17.94
09:07:28.30	02:56:40.0	−28	18.97	18.39	18.05
09:06:19.07	02:59:35.5	1186	19.92	18.81	18.27
09:06:59.84	03:07:05.6	385	19.43	18.86	18.45
09:06:51.15	03:00:04.7	362	19.52	19.05	18.83
09:07:05.23	03:03:18.5	126	20.25	19.43	19.02
09:06:55.76	03:03:15.7	184	20.08	19.52	19.14
09:06:52.43	02:53:09.1	48	20.65	19.71	19.25
09:06:17.87	02:58:02.5	437	20.38	19.76	19.44
09:06:45.28	03:00:37.8	−174	21.05	20.02	19.62
09:06:35.94	03:02:03.7	233	21.42	20.37	20.05
09:06:34.54	03:01:47.9	−687	21.02	20.48	20.08
09:06:46.05	03:00:44.1	−12	21.09	20.59	20.30
09:06:53.43	02:54:17.1	−7	20.64	20.09	19.80
09:06:54.78	03:03:00.6	694	21.18	20.21	19.77
09:07:07.38	02:52:46.0	83	20.97	20.40	20.12
09:07:22.04	03:03:23.2	1968	20.94	20.44	20.09
09:06:54.44	02:57:29.8	392	21.85	20.86	20.39
SDSS data					
09:07:24.35	02:48:25.5	−199	18.22	17.15	16.72
09:07:38.51	02:50:20.2	−282	18.10	17.04	16.57
09:07:10.05	02:52:34.8	155	18.39	17.63	17.18
09:06:55.94	02:52:53.5	−27	18.53	17.42	16.94
09:07:40.86	03:17:35.3	63	....	17.53	17.10

Table B2. SDSS J1045+0420.

RA	Dec.	*RV*	*g*	*r*	*i*
Magellan data					
10:45:48.50	04:20:32.5	0	17.04	15.83	15.36
10:45:47.91	04:20:58.3	838	20.34	19.28	18.86
10:45:48.48	04:21:15.2	−698	21.94	20.84	20.55
10:45:47.49	04:19:40.5	291	19.99	18.88	18.40
10:45:53.28	04:19:51.4	−225	21.52	20.42	20.10
10:45:43.40	04:21:19.5	544	19.57	18.47	18.02
10:45:43.19	04:19:27.7	1556	20.90	19.81	19.37
10:45:53.58	04:19:22.6	689	19.92	18.83	18.38
10:45:50.49	04:18:45.9	387	20.49	19.48	19.02
10:45:44.37	04:22:05.7	574	18.95	17.84	17.38
10:45:41.83	04:19:41.1	368	21.55	20.59	20.16
10:45:43.87	04:22:18.5	−810	21.53	20.63	20.19
10:45:56.36	04:21:25.7	489	19.35	18.28	17.85
10:45:41.52	04:19:13.8	317	19.73	18.62	18.19
10:45:57.30	04:21:03.8	1171	21.22	20.22	19.67
10:45:56.48	04:19:18.3	927	19.83	19.07	18.63
10:45:47.58	04:18:09.1	696	21.22	20.17	19.73
10:45:43.38	04:18:28.3	−806	20.52	19.50	19.03
10:45:58.26	04:21:25.4	−1144	21.09	20.33	19.94
10:45:58.52	04:19:35.4	381	19.13	18.37	17.91
10:45:54.20	04:23:01.9	−587	20.94	19.90	19.53
10:45:55.67	04:22:48.0	−325	21.75	20.77	20.37
10:45:39.83	04:22:27.7	−755	20.77	20.14	19.74
10:45:59.83	04:19:36.8	−4	21.26	20.37	19.96
10:45:42.75	04:17:53.8	−1036	20.95	20.19	19.81
10:45:35.94	04:20:41.2	−169	20.54	19.93	19.69
10:45:45.87	04:24:04.7	−573	21.46	20.46	20.07
10:45:45.92	04:16:35.2	−719	18.97	18.27	17.89
10:45:36.41	04:17:41.0	359	18.21	17.03	16.57
10:45:58.63	04:24:07.3	798	19.44	18.36	17.91
10:45:30.89	04:20:49.7	257	18.74	17.62	17.17
10:45:30.25	04:18:41.3	−543	18.55	17.78	17.38
10:46:07.15	04:23:33.5	1034	19.62	18.46	17.98
10:45:41.60	04:14:44.5	−511	20.82	20.41	20.22
10:45:29.90	04:15:21.4	222	21.77	20.63	20.25
10:46:08.90	04:15:41.2	−220	19.84	18.70	18.18
10:45:26.25	04:24:57.1	−47	19.23	18.14	17.65
10:46:15.95	04:18:18.4	−100	19.98	19.13	18.72
10:46:16.13	04:25:20.3	1140	21.02	20.02	19.44
10:46:01.82	04:12:46.3	−132	21.14	20.10	19.61
10:45:41.36	04:29:03.4	132	19.97	18.88	18.44
10:45:27.41	04:27:29.2	−417	19.96	19.13	18.75
10:45:46.86	04:11:21.2	−367	20.93	20.26	19.96
10:46:15.21	04:27:03.3	791	20.57	19.93	19.67
10:45:35.79	04:29:27.7	301	19.62	18.78	18.34
10:46:26.09	04:22:21.5	224	20.61	19.57	19.09
10:46:16.81	04:13:36.1	−880	20.83	20.06	19.55
10:45:53.73	04:10:40.9	−31	19.55	18.44	17.97
10:46:19.52	04:27:36.5	−151	20.17	19.38	18.93
SDSS data					
10:46:49.97	04:19:38.1	1875	18.63	17.71	17.23
10:46:35.28	04:02:56.3	−13	18.72	17.66	17.19
10:45:02.05	04:01:59.9	−597	18.75	17.59	17.14
10:47:07.62	04:30:29.9	−18	18.85	17.73	17.22
10:47:22.44	04:16:30.1	−102	18.27	17.09	16.48
10:44:46.30	03:53:06.9	−622	17.58	16.42	15.94
10:44:53.91	03:51:28.5	−993	18.59	17.56	17.11
10:43:50.96	04:36:15.3	−855	17.85	16.68	16.20
10:44:00.45	04:42:41.9	−686	18.85	17.68	17.16
10:46:45.93	04:52:46.8	308	18.73	17.70	17.30

Table B3. SDSS J1136+0713.

RA	Dec.	*RV*	*g*	*r*	*i*
Magellan data					
11:36:23.71	07:13:37.5	0	15.90	14.92	14.46
11:36:25.87	07:13:19.5	187	19.45	18.56	18.10
11:36:21.15	07:14:03.7	565	20.88	20.02	19.59
11:36:26.82	07:13:40.7	488	19.68	18.75	18.34
11:36:27.02	07:13:30.6	−239	19.30	18.31	17.92
11:36:22.45	07:12:49.9	698	19.04	18.00	17.53
11:36:26.78	07:14:25.3	102	20.22	19.25	18.86
11:36:18.78	07:13:53.8	−637	19.06	18.07	17.60
11:36:18.67	07:14:00.0	150	18.85	17.84	17.38
11:36:29.45	07:14:22.3	−1030	18.40	17.69	17.30
11:36:29.37	07:14:26.5	117	19.62	18.66	18.16
11:36:16.92	07:12:51.2	−136	20.23	19.33	18.91
11:36:30.28	07:14:30.8	−844	18.31	17.35	16.93
11:36:13.44	07:13:18.6	−228	20.72	19.82	19.40
11:36:34.05	07:13:08.6	−162	19.15	18.16	17.71
11:36:13.93	07:12:34.9	1060	19.19	18.24	18.00
11:36:13.52	07:14:25.2	469	20.75	20.06	19.67
11:36:34.50	07:13:08.7	−387	20.57	19.60	19.18
11:36:30.19	07:15:50.2	−225	19.09	18.61	18.30
11:36:19.95	07:16:11.7	−283	18.97	18.03	17.63
11:36:12.91	07:12:55.5	−302	18.15	17.17	16.75
11:36:31.90	07:15:31.3	−805	20.99	20.37	20.05
11:36:33.70	07:11:55.8	−341	19.34	19.04	18.73
11:36:12.94	07:15:23.5	152	20.26	19.28	18.90
11:36:33.63	07:11:32.5	308	18.45	17.49	17.07
11:36:13.87	07:11:23.3	−425	20.38	19.43	19.01
11:36:37.31	07:12:29.6	−213	18.38	17.51	17.09
11:36:08.36	07:13:45.5	−169	16.50	15.49	15.02
11:36:08.50	07:12:42.8	186	19.34	18.38	17.95
11:36:14.45	07:10:28.6	712	18.97	18.01	17.54
11:36:09.64	07:11:29.2	929	20.63	19.88	19.40
11:36:37.14	07:16:05.8	766	21.69	20.83	20.75
11:36:06.84	07:13:52.4	−243	16.97	15.95	15.50
11:36:39.35	07:11:38.9	410	19.37	18.42	18.00
11:36:05.22	07:11:57.8	134	17.59	16.60	16.15
11:36:41.66	07:16:41.6	−148	20.19	19.19	18.70
11:36:48.67	07:13:09.2	−983	19.51	18.62	18.15
11:36:42.03	07:18:13.9	−26	17.87	16.87	16.42
11:35:57.72	07:14:19.4	−708	21.12	20.41	20.16
11:36:50.22	07:15:45.7	234	20.78	19.87	19.51
11:36:31.27	07:20:38.1	190	19.72	18.83	18.27
11:35:59.90	07:08:35.5	480	18.82	18.36	18.04
11:36:48.73	07:19:39.8	183	18.95	18.12	17.67
11:37:01.13	07:12:29.1	−417	19.07	18.45	18.12
11:35:45.01	07:15:41.4	−64	21.36	20.56	20.23
11:36:46.73	07:23:00.2	−28	19.60	18.82	18.36
11:35:36.83	07:09:06.3	805	18.28	17.35	16.94
11:35:34.30	07:10:53.4	852	19.31	18.32	17.88

Table B4. SDSS J0856+0553.

RA	Dec.	*RV*	*g*	*r*	*i*
Magellan data					
08:56:40.72	05:53:47.3	0	16.05	15.02	14.57
08:56:40.71	05:53:04.0	651	19.83	18.90	18.44
08:56:43.68	05:53:33.8	−104	19.43	18.35	17.99
08:56:38.61	05:52:52.9	11	19.56	18.62	18.19
08:56:40.09	05:54:52.5	67	19.40	18.42	18.00
08:56:38.75	05:52:28.5	−634	20.72	19.80	19.35
08:56:34.91	05:54:17.7	−91	20.13	19.26	18.83
08:56:40.57	05:55:20.5	−1226	18.89	18.31	17.91
08:56:47.32	05:53:59.5	213	20.15	19.24	18.81
08:56:41.34	05:55:34.4	80	18.88	17.88	17.44
08:56:37.31	05:51:59.2	−803	18.60	17.64	17.18
08:56:38.04	05:51:49.3	−182	19.78	18.85	18.41
08:56:34.22	05:55:40.4	−420	19.58	18.81	18.40
08:56:45.66	05:51:36.2	−393	20.66	19.87	19.45
08:56:44.69	05:51:28.0	−646	19.35	18.41	17.98
08:56:35.97	05:51:32.2	−588	18.87	17.93	17.47
08:56:29.10	05:54:39.6	−554	20.14	19.30	18.93
08:56:28.55	05:53:55.1	141	21.56	20.67	20.37
08:56:47.62	05:56:30.8	1119	20.85	19.97	19.56
08:56:52.51	05:55:10.4	107	19.58	18.62	18.19
08:56:29.49	05:51:40.9	420	19.60	18.72	18.30
08:56:39.61	05:50:11.6	154	19.65	18.74	18.30
08:56:30.27	05:51:07.8	−418	21.13	20.34	19.86
08:56:51.01	05:56:34.2	−175	19.55	18.60	18.22
08:56:31.75	05:50:43.6	208	20.62	19.59	19.22
08:56:23.73	05:53:19.9	275	18.86	17.83	17.33
08:56:25.67	05:56:04.2	−390	21.24	20.41	20.01
08:56:24.24	05:49:37.9	39	20.54	19.65	19.28
08:57:02.52	05:56:26.5	522	19.75	19.49	19.27
08:56:35.46	05:47:18.1	−177	19.69	19.24	18.94
08:57:03.70	05:57:24.2	−166	19.53	18.56	18.03
08:56:11.67	05:52:55.9	−625	21.38	20.45	20.13
08:56:59.40	05:48:07.3	730	18.98	18.04	17.59
08:56:50.78	05:46:47.5	−67	19.72	18.78	18.37
08:56:56.09	05:47:22.9	−594	19.67	18.91	18.51
08:56:29.71	05:46:22.4	−178	21.59	20.63	20.14
08:57:12.61	05:51:31.1	171	20.81	20.16	19.77
08:57:13.75	05:52:34.4	187	19.70	18.98	18.51
08:56:22.76	05:46:30.2	449	19.62	18.73	18.30
08:56:32.03	05:45:00.2	820	20.47	19.71	19.43
08:56:13.22	05:59:44.9	−335	20.56	20.12	19.86
08:57:08.63	05:59:50.9	184	20.13	19.15	18.80
08:57:17.72	05:54:32.4	−443	19.33	18.52	18.04
08:56:02.99	05:54:52.1	243	21.64	20.70	20.47
08:56:39.86	06:04:05.9	−273	20.97	20.37	20.07
08:57:04.71	05:44:16.1	−515	20.50	19.89	19.63
08:55:53.45	05:54:04.5	220	20.84	19.75	19.32
08:56:49.02	05:40:39.5	1068	21.93	20.94	20.86
SDSS data					
08:56:54.63	05:49:35.6	291	18.42	17.54	17.11
08:56:55.79	05:56:29.8	926	18.03	17.14	16.73
08:56:30.82	05:57:20.6	329	17.96	17.06	16.65
08:56:41.49	05:51:37.8	1394	18.31	17.27	16.81
08:56:39.80	05:55:26.2	877	18.51	17.53	17.09
08:56:50.01	05:48:38.7	152	17.73	16.75	16.32
08:56:25.57	05:58:04.6	−275	18.50	17.52	17.09
08:56:23.21	05:49:49.4	307	17.74	16.69	16.22
08:57:06.03	05:51:54.4	−190	18.19	17.24	16.80
08:56:07.76	05:54:45.0	264	17.22	16.27	15.85
08:56:33.00	06:01:50.3	−199	17.63	16.65	16.21
08:57:09.34	05:48:26.5	307	17.74	16.73	16.27
08:56:07.24	05:55:53.2	87	17.92	16.94	16.52
08:57:25.80	05:57:57.8	397	17.29	16.35	15.93

Table B5. SDSS J0856+0553 cont.

RA	Dec.	*RV*	*g*	*r*	*i*
SDSS data					
08:56:49.61	05:41:33.5	128	18.59	17.70	17.29
08:55:57.99	05:52:14.8	−24	17.51	16.56	16.11
08:55:42.60	05:55:42.5	−84	18.26	17.31	16.85
08:55:50.98	06:03:31.5	−147	17.21	16.55	16.15
08:57:25.69	05:41:41.1	35	17.54	16.52	16.07
08:55:05.94	05:58:06.8	1287	17.99	17.21	16.77
08:56:42.63	05:28:19.4	109	18.71	17.67	17.17
08:58:17.91	06:05:34.2	221	18.31	17.73	17.40
08:58:30.66	05:49:31.8	−111	17.99	16.98	16.50
08:55:08.10	06:09:53.8	−76	17.66	17.07	16.54
08:58:33.14	05:48:08.1	199	18.04	16.95	16.47
08:58:45.57	05:51:03.5	183	17.31	16.46	15.98
08:58:03.69	06:19:04.6	384	18.36	17.75	17.49
08:58:08.74	06:18:16.4	−146	17.83	16.80	16.31
08:58:05.20	06:20:12.7	−65	17.56	16.82	16.39
08:54:35.32	05:39:41.9	28	17.19	16.26	15.82
08:54:29.11	05:43:39.2	1411	18.46	17.55	17.17
08:57:29.42	06:26:56.2	−144	18.48	17.71	17.32
08:55:17.80	05:24:53.4	720	17.71	16.94	16.53
08:56:34.13	06:29:39.7	240	18.03	17.20	16.67
08:56:12.98	06:33:29.7	1127	18.64	18.09	17.66
08:56:48.24	06:34:32.4	856	18.67	17.82	17.30
08:55:27.47	06:30:23.8	1409	16.84	16.22	15.84
08:56:38.82	05:53:33.1	−150	18.85	17.83	17.35

Table B6. SDSS 1017+0156.

RA	Dec.	*RV*	*g*	*r*	*i*
Magellan data					
10:17:45.57	01:56:45.8	0	16.36	15.28	14.78
10:17:42.06	01:53:47.8	−747	18.18	17.16	16.74
10:17:55.52	01:54:34.8	445	19.06	17.97	17.50
10:17:38.88	01:53:28.9	327	19.12	18.05	17.61
10:17:43.48	01:57:56.0	−1298	19.11	18.07	17.64
10:17:55.90	01:55:16.4	80	19.36	18.59	18.24
10:17:47.14	01:54:44.6	279	19.70	18.67	18.23
10:17:32.07	01:55:29.6	−459	21.00	19.92	19.43
10:18:00.06	01:56:34.6	−193	20.98	20.00	19.64
10:17:39.44	01:53:44.2	−759	21.49	20.99	20.69
10:18:36.01	02:01:58.1	1179	19.08	18.07	17.55
10:18:14.74	01:59:15.8	295	19.00	18.43	18.01
10:18:16.78	02:06:01.8	1365	19.40	18.62	18.19
10:17:46.32	02:02:13.8	157	20.08	19.30	18.80
10:18:00.24	02:00:51.3	350	20.27	19.61	19.23
10:18:33.57	01:55:12.5	253	20.32	19.63	19.25
10:18:32.17	01:59:50.0	1508	20.81	20.11	19.73
10:17:28.87	01:55:16.3	−658	21.26	20.54	20.19
10:17:24.90	01:45:54.4	982	21.82	20.72	20.23
10:17:51.72	01:57:27.6	−513	19.15	17.99	17.45
10:17:45.08	01:54:37.0	−198	19.26	18.21	17.80
10:17:42.79	01:57:08.1	307	19.41	18.32	17.87
10:17:55.73	01:59:27.6	−300	20.63	19.60	19.12
10:17:57.54	01:55:13.0	562	21.50	20.57	19.99
10:18:12.59	01:51:42.0	137	20.31	19.26	18.76
10:18:12.71	01:52:57.3	93	20.23	19.66	19.41
10:17:04.75	01:52:47.4	1177	20.57	19.89	19.60
10:18:17.90	01:57:32.7	309	20.54	19.91	19.44
10:17:32.26	01:52:26.3	97	21.78	20.74	20.45
10:16:51.08	01:56:04.0	257	....	....	....
SDSS data					
10:17:16.15	02:16:22.6	1117	17.41	16.38	15.91
10:17:43.32	01:38:06.4	1185	17.97	17.68	17.39
10:17:45.73	02:14:06.7	936	18.44	17.40	16.97
10:18:37.23	02:03:42.9	1221	17.94	16.83	16.31
10:18:50.50	02:04:22.8	1124	18.51	17.42	16.93
10:19:01.74	01:56:19.9	−87	18.37	17.55	17.06

Table B7. RX J1256.0+2556.

RA	Dec.	*RV*	*g*	*r*	*i*
Gemini data					
12:56:02.27	25:56:37.2	0	18.22	16.76	16.29
12:55:54.88	25:57:59.0	−1228	22.09	....	20.99
12:55:55.59	25:56:33.8	−1111	21.00	....	19.40
12:56:01.97	25:56:40.4	−1029	20.33	....	18.75
12:55:55.55	25:57:10.8	−876	21.18	....	19.56
12:55:51.19	25:57:33.5	−817	22.74	....	21.35
12:56:02.55	25:56:50.0	−790	20.68	....	19.37
12:55:54.98	25:58:24.8	−612	20.13	....	18.60
12:56:09.04	25:55:47.5	−479	20.62	....	19.57
12:56:08.88	25:55:57.9	−411	20.38	....	18.98
12:55:54.33	25:56:14.5	−187	20.71	....	19.53
12:55:57.90	25:58:19.5	−148	19.25	....	17.63
12:56:01.09	25:57:02.2	−121	20.61	....	18.94
12:56:03.29	25:54:37.1	75	19.84	....	18.10
12:56:00.57	25:57:22.8	138	21.61	....	20.06
12:56:02.34	25:55:14.2	187	20.50	....	18.91
12:56:01.73	25:55:18.3	229	19.91	....	18.45
12:56:01.70	25:56:28.9	259	20.71	....	19.41
12:55:54.43	25:58:10.4	276	21.94	....	20.38
12:56:02.67	25:56:32.8	479	20.25	....	18.68
12:56:09.34	25:56:09.6	520	22.06	....	20.35
12:56:03.17	25:56:24.5	749	22.47	....	19.98
12:56:00.86	25:55:21.4	775	21.28	....	19.90
SDSS data					
12:55:04.55	26:02:54.7	−982	18.87	17.50	16.97
12:54:53.39	25:50:56.7	−18	18.52	17.12	16.59
12:54:38.82	25:52:13.5	−825	18.90	17.46	16.96
12:56:07.18	25:57:23.9	759	20.33	....	18.65
12:56:03.48	25:57:02.2	−921	20.96	....	19.20
12:55:53.01	25:57:23.9	−872	19.93	....	18.04
12:55:56.30	25:55:56.3	152	....	....	....
12:56:02.24	25:56:32.0	565	19.68	....	17.82

Table B8. RX J1331.5+1108.

RA	Dec.	*RV*	*g*	*r*	*i*
Gemini data					
13:31:29.7	11:07:57	0	16.36	15.40	14.95
13:31:33.4	11:05:46	51	25.12	22.16	22.07
13:31:22.5	11:07:15	359	19.88	19.57	19.33
13:31:34.6	11:08:02	666	23.14	21.31	20.53
13:31:24.0	11:08:20	−309	18.71	17.84	17.46
SDSS data					
13:31:36.4	11:13:02	495	17.07	16.47	16.11
13:31:41.5	11:06:45	−328	18.03	17.25	16.84
13:31:14.3	11:08:24	−88	17.79	16.92	16.45
13:31:09.9	11:05:20	163	17.15	16.28	15.91
13:31:26.0	11:05:32	412	18.25	17.55	17.10

This paper has been typeset from a TEX/LATEX file prepared by the author.